The effects of post-condensation exchange on the isotopic composition of water in the atmosphere

Robert D. Field[1], Dylan B. A. Jones[1] and Derek P. Brown[2]

[1]Department of Physics, University of Toronto, Toronto, Canada

[2]Department of Atmospheric and Oceanic Sciences and Cooperative Institute for Research in Environmental Sciences, University of Colorado, Boulder, Colorado, USA

Running title: Isotopes and post-condensation exchange

Key words: Stable water isotopes, moisture recycling, rainfall evaporation, Tropospheric Emissions Spectrometer, temperature effect.

Abstract

We conducted experiments with an atmospheric general circulation model to determine the effects of non-Rayleigh, post-condensation exchange (PCE) on the isotopic composition of water in the atmosphere. PCE was found to universally deplete vapor of heavy isotopes, but had differential effects on the isotopic composition of precipitation. At low latitudes, local PCE with fresh vapor at the surface enriches precipitation in heavy isotopes, particularly during light rainfall. When rainfall is heavy, PCE tends to deplete vapor and precipitation of heavy isotopes via atmospheric moisture recycling, supporting recent interpretations of vapor isotope measurements from satellites, particularly over the Asian Monsoon region. In the extratropics, PCE causes local enrichment of precipitation, which is often entirely offset by upstream PCE depletion of the source vapor, resulting in a net depletion in local precipitation. The transition from net enrichment to net depletion is controlled by the transition from rain to snow-dominated precipitation. Surprisingly, this transition was also found to influence the temperature effect. In regions with a strong seasonal mix of rain and snow, such as Europe, the temperature effect appears to be controlled by PCE rather than Rayleigh depletion.

1. Introduction

Dansgaard [1954] identified the origin of the water vapor and the amount of previous rainfall from the air mass as the dominant controls on the isotopic composition of atmospheric moisture. These formed the basis of the Rayleigh distillation model [*Dansgaard*, 1964], which is the most important concept in isotope hydrometeorology, and explains much of the observed spatial variation in the isotopic composition of precipitation. According to this model, the heavy isotopes (isotopologues) $H_2{}^{18}O$ and HDO condense preferentially relative to the light isotope $H_2{}^{16}O$, causing the progressive isotopic depletion of the air mass at it loses moisture. In its most basic form, the ratio R_v of heavy to light isotopes in the residual vapor following a phase change is described by

$$R_v = R_o f^{(\alpha-1)} \qquad \textbf{(1)}$$

where R_o is the initial isotopic ratio of the vapor after evaporation from the ocean surface, f is the fraction of original vapor remaining, and α is a temperature-dependent fractionation factor, greater for ice deposition than for condensation [*Majoube*, 1971a; b]. Rayleigh theory dictates the instantaneous removal of condensate following a phase change, and hence the isotopic composition of condensate is by extension controlled by the same 'pre-history'. Isotopic composition is expressed as the normalized difference between the measured and VSMOW ratios using δ-notation in units of permil (‰). $H_2{}^{18}O$ composition, for example, is expressed as:

$$\delta^{18}O = \left(\frac{R - R_{VSMOW}}{R_{VSMOW}} \right) \times 10^3 .$$

Rayleigh models with varying degrees of complexity have been widely used to interpret isotopic observations. *Dansgaard* [1964] used the model to explain the observed poleward depletion of precipitation $\delta^{18}O$, and its positive relationship with surface temperature, referred to as the "temperature effect", which results primarily from the temperature-dependence of saturation vapor pressure. The model has been widely used to interpret the isotopic depletion of precipitation toward the continental interiors, for example, in Europe [*Rozanski et al.*, 1982; *Sonntag and Schoch-Fischer*, 1985], northeast Asia [*Kurita et al.*, 2004; *Yamanaka et al.*, 2007] and in southeast Asia [*Araguas-Araguas et al.*, 1998]. More sophisticated, Rayleigh-like distillation models have been applied in Lagrangian and Eulerian frameworks, whereby distillation occurs over moisture trajectories computed from reanalysis fields and is used to characterize transport pathways under different circulation regimes (eg. *Yoshimura et al.* [2003], *Sodemann et al.* [2008]).

Regardless of their complexity, these models assume that condensate is immediately removed upon formation [*Jouzel et al.*, 1997], locking in the isotopic composition of precipitation. Complicating this assumption is the post-condensation exchange (PCE) that occurs between condensate and vapor, which *Dansgaard* [1954] recognized. Raindrops falling into unsaturated air will partially or fully re-evaporate, changing the isotopic composition of both the raindrops and surrounding vapor [*Friedman et al.*, 1962; *Stewart*, 1975; *Celle-Jeanton et al.*, 2004; *Risi et al.*, 2010a]. Under low humidity conditions, partial droplet re-evaporation can enrich precipitation $\delta^{18}O$ [*Dansgaard*, 1954; *Araguas-Araguas et al.*, 1998; *Gat*, 2000; *Stern and Blisniuk*, 2002; *Danis et al.*, 2006; *Strong et* *al.*, 2007], but also contribute more depleted moisture into the ambient environment, depleting subsequent precipitation [*Gedzelman and Arnold*, 1994; *Lawrence et al.*, 2004; *Risi et al.*, 2008]. Similarly, raindrops falling into saturated layers will tend to equilibrate isotopically with the surrounding vapor [*Friedman et al.*, 1962; *Lee et al.*, 2007], which may be isotopically different than the vapor from which the raindrops originally formed [*Kavanaugh and Cuffey*, 2003]. PCE, in the form of either re-evaporation or equilibration, is limited to liquid phase precipitation and does not occur for ice, or rather, occurs at time scales much longer than the descent of condensation [*Friedman et al.*, 1962; *Ciais and Jouzel*, 1994; *Gonfiantini et al.*, 2001; *Friedman et al.*, 2002; *Tian et al.*, 2003; *Celle-Jeanton et al.*, 2004]. Re-evaporation and atmospheric moisture recycling are often invoked to explain deviations between $\delta^{18}O$ observations and simple Rayleigh-type model predictions [*Brown et al.*, 2008; *Feng et al.*, 2009], or to explain uncertainty in a relationship between a climatic variable of interest and $\delta^{18}O$ [*Etien et al.*, 2008]. Furthermore, through the detailed diagnosis of isotopically-equipped single column and idealized microphysical models, *Risi et al.* [2008] and *Lee and Fung* [2008] identified PCE as the most important factor contributing to the rainfall 'amount effect', the negative relationship between precipitation amount and its isotopic composition.

Few studies have been conducted to assess the importance of PCE on the isotopic composition of precipitation at a global scale, although steps have been made recently, motivated by the availability of vapor δD measurements from satellites. *Worden et al.* [2007] found that over the tropical lower troposphere, δD measurements from the Tropospheric Emissions Spectrometer (TES) satellite instrument were more depleted than would be expected from Rayleigh depletion. Using an idealized model of vapor isotopic composition, *Worden et al.* [2007] were able to explain these observations using different fractions of rainfall re-evaporation. *Brown et al.* [2008] subsequently examined tropical continental convection regions in detail, and suggested that the occurrence of overly depleted δD observations were attributable to intensive upstream atmospheric moisture recycling. Using experiments with an atmospheric GCM equipped with stable water isotope tracers, *Wright et al*. [2009] found that with re-evaporation in the model disabled, the δD composition of vapor was less-depleted by up to 50‰, constituting a non-negligible proportion of vapor depletion attributable not to Rayleigh depletion, but rather to PCE, consistent with the vapor recycling hypotheses used to explain the depleted TES measurements. *Noone and Sturm* [2010] conducted a series of experiments to illustrate the partitioning of precipitation $\delta^{18}O$ between fractionation during surface evaporation, convective condensation, stratiform condensation and post-condensation equilibration. For the latter, they showed that equilibration tended to enrich precipitation at low-latitudes, but deplete precipitation at high latitudes.

Following these studies, the goal of this work was to further quantify the effects of PCE on the isotopic composition of precipitation and vapor using an isotopically-equipped GCM, particularly in the context of the rapid growth of vapor isotope data from satellites. Many GCM-based studies have examined the relationship between $\delta^{18}O$ and different meteorological parameters, such as local temperature [*Hoffmann et al.*, 1998; *Cole et al.*; *Noone and Simmonds*, 2002; *Vuille and Werner*, 2005; *Schmidt et al.*, 2007], regional moisture balance [*Lee et al.*, 2007], or atmospheric circulation [*Werner and Heimann*, 2002; *Vuille and Werner*, 2005; *Schmidt et al.*, 2007; *Field*, 2010]. Although GCM-based, these studies are similar to observational analyses in diagnosing controls on isotopic composition from a control simulation, and not experimental in the sense of systematically manipulating certain processes within the model. Indeed, *Helsen et al.* [2007] and *Masson-Delmotte et al.* [2008] state that one disadvantage of a GCM is that its complexity makes it difficult to separate the influence of different fractionation processes. In this regard, the experimental approaches of *Wright et al.* [2009] and *Noone and Sturm* [2010] were unique; the experiments conducted here follow in that context.

2. Experimental design

In this study, we conducted simulations with the NASA Goddard Institute for Space Studies (GISS) ModelE GCM [*Schmidt et al.*, 2005; *Schmidt et al.*, 2006]. ModelE is one of several GCMs which include tracers of stable water isotopes, with fractionation between the light $H_2^{16}O$ isotope and the heavy $HD^{16}O$ and $H_2^{18}O$ isotopes at all stages of the hydrological cycle, from evaporation from the land and ocean surfaces, to condensation and PCE in clouds. For PCE, full isotopic equilibration is applied for stratiform precipitation, and 50% equilibration is applied for convective precipitation, reflecting the faster rates of descent and larger droplet sizes in convective systems [*Schmidt et al.*, 2005]. The model was run at a moderate resolution of 4° x 5° in the horizontal and 20 vertical levels, based on the M20 simulation in *Schmidt et al.* [2005]. All simulations were run for 45-years with annually-varying prescribed SSTs from HadISST 1.1 dataset [*Rayner et al.*, 2003] starting in 1953, although for the purposes of this experiment, the choice of simulation period was arbitrary and not intended to reproduce observed isotopic measurements.

The control run (CTRL) had all isotopic processes enabled, and was comparable to the CONT run of *Schmidt et al.* [2005], or the CTL run in *Wright et al.* [2009]. The INIT run was an experimental simulation with fractionation occurring during initial condensation only, and without any fractionation during PCE, namely equilibration or condensate evaporation, analogous to the LSC-SS run in *Wright et al.* [2009]. As in that study, we interpret INIT run as a Rayleigh distillation model, but with realistic advection and mixing of moisture. We took a slightly different approach than the *Wright et al.* [2009] experiments, where all tracer from re-evaporation was eliminated. In the INIT experiment, tracers are transferred between reservoirs, and therefore conserved, but with no fractionation (i.e. fractionation factors set to 1) and, consequently, with no isotopic signature left by PCE processes. Like *Wright et al.* [2009], the changes are limited to off-line tracers, and core prognostic quantities are identical across experiments, unlike 'on-line' re-evaporation experiments [*Bacmeister et al.*, 2006; *Maloney*, 2009] where changes to re-evaporation were applied to the core prognostic processes and can affect the model's dynamics through heat exchange as water changes phase.

Our analysis was limited to first-order isotopic quantities, which are more accurately simulated than the second-order deuterium excess in ModelE [*Schmidt et al.*, 2007] and other GCMs [*Yoshimura et al.*, 2008; *Noone and Sturm*, 2010]. Direct comparison of the GCM results was made to precipitation $\delta^{18}O$ observations from the Global Network of Isotopes in Precipitation (GNIP) [*IAEA*, 2001]. From the GNIP stations, only stations with 5 or more years worth of isotope data were used in the analysis. This GNIP data were supplemented with other data for under-sampled regions, which had sub-annual resolution. Over Russia, recently available 5-year data for 12 stations from *Kurita et al.* [2004] were included. Data was also included for Greenland, at the Summit [*Hastings et al.*, 2004] and NGRIP [*Shuman et al.*, 2001] sites, and for Antarctica at South Pole [*Aldaz and Deutsch*, 1967], Vostok [*Ekaykin*, 2003] and Law Dome [*van Ommen and Morgan*, 1997].

We also conducted a preliminary comparison between our GCM experiments and δD observations from TES reported in *Brown et al.* [2008]. The TES instrument is a Fourier transform spectrometer measuring infrared emissions over the 650-3050 cm^{-1} range [*Beer et al.*, 2001]. The TES HDO retrieval is based on lines in the 1150-1350 cm^{-1} range, and has peak sensitivity at 700 hPa, with a precision of 1% to 2%, which decreases at higher latitudes [*Worden et al.*, 2006]. Due to a systematic bias in line strength, a -5% correction was accounted for in the HDO concentrations in *Worden et al*. [2006] and *Brown et al*. [2008], which results in an additional δD depletion of ~40-50 ‰. Because of the coarse vertical resolution of the TES retrievals, the measurements reflect a free-tropospheric average rather than a true tropospheric profile. In our analysis we therefore average the modeled fields between 470 and 847 hPa in order to accommodate this feature of the TES retrieval, and to compare more accurately the model with the TES data.

3. Global overview

3.1. Basic features of CTRL

The seasonal distributions of temperature and precipitation for CTRL are shown in Figure 1, both of which, as expected, were in good agreement with the M20 simulations of *Schmidt et al.* [2006]. The annual mean surface air temperature was 14.3°C (14.4°C in their M20), the precipitation rate was 3.0 mm/day (2.96 mm/day in their M20), and the 847hPa specific humidity q was 6.3 g kg^{-1} (6.5 g kg^{-1} for their 850 hPa q). The mean annual precipitation $\delta^{18}O$ was -7.3‰, compared to their -7.5‰.

Figure 2 shows the seasonal distribution of precipitation $\delta^{18}O$ for CTRL. The least depleted precipitation $\delta^{18}O$ occurs over the dry subtropical anticyclones, with values close to the ocean water standard. At low latitudes, the most depleted precipitation $\delta^{18}O$ is associated with heavy rainfall (Figure 1), most notably the continental convective regions of northern South America and southern Africa during the DJF wet season. In absolute terms, the most depleted values occur over the polar ice caps, with a minimum of -61‰ over East Antarctica during JJA, and in the northern hemisphere with -37‰ over Greenland during DJF. Seasonal vapor $\delta^{18}O$ at the surface and mid-troposphere are shown in Figure 3. The gradients in surface vapor $\delta^{18}O$ generally follow those of precipitation $\delta^{18}O$, but the precipitation $\delta^{18}O$ is greater on average by 10‰, corresponding to the fractionation that occurs as the vapor condenses initially. The mid-tropospheric vapor $\delta^{18}O$ shows a further depletion from the surface vapor, and sharper low-latitude gradients between dry and humid regions. Throughout the depth of troposphere (Figure 4), the vapor $\delta^{18}O$ is more depleted in each hemispheric winter, a seasonal shift similar to precipitation $\delta^{18}O$.

3.2.Changes in $\delta^{18}O$ in the absence of PCE

The primary global feature of the precipitation $\delta^{18}O$ difference maps for INIT is the separation between regions of net increase at high latitudes and decrease at low latitudes in the absence of PCE (Figure 5). For DJF, the high-latitude increases are relatively constant, reaching 7 ‰ over the North American interior and 5 ‰ over the Eurasian interior. During JJA, the precipitation $\delta^{18}O$ increase in the NH has retreated poleward, replaced with a net decrease over much of Eurasia and North America. At low latitudes, there is an inverse relationship between the magnitude of the decrease in precipitation $\delta^{18}O$ for INIT and precipitation amount (Figure 1). The strongest decreases of up to 8‰ occurred over the dry, subtropical anticyclones, and the weakest decreases over regions of heavy precipitation. Regions where the decrease is weakest shift seasonally with heavy rainfall, such as the ITCZ, continental convective regions of South America and Africa, and the Asian Monsoon region.

The increases at high latitudes in INIT show where PCE has a net-depleting effect, and the decreases at low latitudes show where PCE has a net enriching effect. This separation is consistent with the results of the similar PCE experiment conducted by *Noone and Sturm* [2010]. Common to the results of both experiments, in the annual mean, are the greatest enriching effects occurring over the dry subtropics and the pronounced depleting effects over the Asian Monsoon region, and over west-central South America. The magnitude of the difference is larger here at both high and low latitudes, which is likely due to the slightly stronger equilibration rates in GISS for both stratiform and convective condensate compared to *Noone and Sturm* [2010], and also to ModelE possibly having stronger condensate evaporation compared to other GCMs [*Wright et al.*, in press].

A mechanistic explanation for this separation follows from *Gedzelman and Arnold* [1994], *Risi et al.* [2008], and *Noone and Sturm* [2010]. Partial re-evaporation of raindrops will enrich the raindrops, but transfer depleted vapor into the surrounding air. The situation is similar for raindrops equilibrating with vapor that is less depleted than that from which precipitation originally formed. If either type of PCE has occurred, subsequent condensate forming from this vapor reservoir will be more depleted than if PCE had not occurred. At a given precipitation site, therefore, condensate can be enriched by local PCE, but that may be offset, or exceeded, by the depletion that PCE causes to the upstream vapor reservoir. The INIT experiment identifies the regions where any local enrichment of precipitation from PCE is exceeded by upstream vapor depletion from PCE.

In this regard, the phase of precipitation is critical: PCE occurs between vapor and liquid condensate but not between vapor and ice [*Friedman et al.*, 1962; *Ciais and Jouzel*, 1994; *Gonfiantini et al.*, 2001; *Friedman et al.*, 2002; *Tian et al.*, 2003; *Celle-Jeanton et al.*, 2004]. When solid condensate forms and falls as precipitation, there is no enrichment from local PCE, only the vapor-depleting effects from any PCE for upstream precipitation that occurred as liquid. To see the importance of the phase of precipitation, the fraction of precipitation falling as snow is shown at the 0.1 and 0.9 contour levels in Figure 5. Equatorward of the 0.1 contour, most precipitation falls as rain, and poleward of the 0.9 contour, most falls as snow. Particularly for DJF, the transition from rain- to snow-dominated precipitation across 40°N provides a strong demarcation in the INIT run between regions of low-latitude net precipitation $\delta^{18}O$ decrease and high-latitude net increase. Equatorward of this transition zone, rainfall will exchange isotopically with freshly evaporated ocean water, whereas poleward of this transition zone, the depleting effects of PCE on vapor $\delta^{18}O$ have been locked in.

Unlike precipitation $\delta^{18}O$, vapor $\delta^{18}O$ always increased in the absence of PCE (Figure 6), as was seen in *Wright et al.* [2009] for δD, but with considerable spatial variation. For surface vapor $\delta^{18}O$ (Figure 6) in INIT during DJF, there is an increase over land in the extra-tropics, and a weaker increase over ocean. At low latitudes, there are stronger increases in surface vapor $\delta^{18}O$ in regions of heavy precipitation, corresponding to the weak decrease in precipitation $\delta^{18}O$ for INIT.

The zonal structure of the vapor $\delta^{18}O$ increases for INIT reflect basic features of the mean zonal circulation during different seasons (Figure 7), and also precipitation phase. The strongest vapor $\delta^{18}O$ increase for INIT during DJF is in the southern extra-tropical free-troposphere, with an increase of ~10‰ between 300 and 400 hPa poleward of 40°S. In the NH, the positive $\delta^{18}O$ change for INIT is largely constant poleward of 40°N, and weaker than in the SH. At these latitudes in the NH, vapor depletion from PCE has occurred during liquid phase precipitation in the low-mid latitudes, and becomes locked in at the transition to snow-dominated precipitation, resulting in little zonal gradient poleward of 40°N. Over the tropics, the maximum in the mid-troposphere increase for INIT in the ascending region between 0° and 20°S is associated with the vigorous moisture exchange of the tropical rainfall belts. In the descending region centred on 20°N, the increase in vapor $\delta^{18}O$ for INIT is weakest near the surface, where the air is humid (Figure 8) and dominated by isotopically fresh evaporate from the ocean surface. This difference increases above the boundary layer to ~ 5‰ at 500 hPa, which reflects the mixing of air into the subtropics from subsidence, equatorward return flow, and convective detrainment [*Pierrehumbert*, 1998], which has undergone more upstream PCE depletion.

During JJA, the structure of the zonal mean change for INIT mirrors that during DJF. There is a much stronger JJA increase in the NH extratropics than seen in the southern hemisphere during DJF, due to the more poleward shift in the snowline (Figure 5), and consequent increase in PCE over the NH. In this respect, we note that the peak of the annual-mean NH increase in *Wright et al.* [2009] over the North Pole in their LSC-SS experiment was a muted version of the JJA increase in Figure 7.

3.3. Comparisons to GNIP

There were large differences between modeled and observed precipitation $\delta^{18}O$ (Table 1, Figure 9) for the two experiments. For the CTRL run during DJF, there was a strong correlation of r = 0.93 between the precipitation $\delta^{18}O$ observations and that from the nearest grid cell in ModelE, with an overall model bias of -1.0‰ toward more depleted values, and a root-mean square error (RMSE) of 3.2‰.

For INIT, the correlation was reduced to r = 0.81, the bias increased to -2.5‰ , and, most notably, the RMSE increased to 5.9‰. Similar changes were observed during JJA. During both seasons, the overall bias for INIT reflects a strong negative bias for less depleted precipitation $\delta^{18}O$ offset by a positive bias for more depleted values. For observed precipitation $\delta^{18}O$ values > -15‰, modeled precipitation $\delta^{18}O$ is over-depleted, with only a weak slope. For observed precipitation $\delta^{18}O$ values < - 20‰ , there is a constant under-depletion bias in the GCM, but a strong Rayleigh-driven slope. As in Figure 5, the difference for INIT has been locked in poleward of the snowline, represented by the positive offset and absence of a decreasing gradient below the snow line.

The strong correlations between the GCM and observations were highly dependent on the inclusion of the Antarctic and Greenland data, particularly during the boreal summer (Table 1). Without these observations, the JJA correlation was reduced to r = 0.72 for CTRL, and r = 0.37 for INIT: in the absence of data from strong Rayleigh depletion regimes, the contributions of PCE are much more important in explaining the observed variation of precipitation $\delta^{18}O$. Furthermore, and as *Vuille et al.* [2005] state, such a comparison should be taken cautiously given the uneven distribution of GNIP stations, differences in the period and length of reporting, and mix of observation types between snow gauges, snow pits, and shallow cores.

4. Regional comparisons

The changes for INIT varied strongly across different climate regimes and seasons, and are examined in the following sections for the wet tropics, the Asian monsoon region, the dry tropics/subtropics, and the extra-tropics.

4.1. Wet tropics

At low latitudes, the spatial variation of the decrease in precipitation $\delta^{18}O$ (Figure 5) results from differing effects of PCE aloft and at the surface. In the convective column, PCE will tend to deplete precipitation $\delta^{18}O$ through atmospheric recycling of re-evaporated and equilibrated vapor, as described in the detailed single-column analysis of *Risi et al.* [2008]. At the surface, by contrast, PCE will tend to enrich precipitation $\delta^{18}O$ via exchange with fresh, relatively un-depleted near-surface vapor. The near-uniform decrease in precipitation $\delta^{18}O$ for INIT reflects the PCE with this near-surface vapor, but is offset in heavy precipitation regions by the recycling of water vapor that occurs during rainfall. The weaker effect of PCE for heavy precipitation is also consistent with the suggestion [*Lee et al.*, 2007; *Scholl et al.*, 2009] that heavy precipitation, with its larger-diameter raindrops, will undergo less exchange than lighter raindrops, and therefore undergo less enrichment via PCE with surface evaporate. In regions of heavy precipitation over land, there are in fact isolated grid cells for which a net decrease in precipitation $\delta^{18}O$ occurs for INIT, reflecting the dominance of depletion from recycling in the convective column over enrichment effects occurring near the surface. This dominance does not occur over the same regions during the dry JJA season due to the absence of strong convective recycling. There is in fact a strong decrease of up to 8 ‰, which is likely due also to the absence of PCE with vapor transpired from vegetation, which undergoes no isotopic fractionation from soil water to vapor, and is therefore highly un-depleted [*Gat and Matsui*, 1991].

The depleting effects of PCE in the column are seen more clearly in the changes to vapor $\delta^{18}O$ for INIT, particularly over southern Africa and northwestern South America during DJF (Figure 6). In these regions, the increase in vapor $\delta^{18}O$ extended through to the mid-troposphere over the continental 'tropical chimneys', and reflects the intensity of deep convection and subsequent atmospheric vapor recycling in those regions. We note also that when the 470hPa vapor $\delta^{18}O$ difference maps of Figure 6 are averaged annually (not shown), the peaks in vapor $\delta^{18}O$ increases over northwestern South America and equatorial Africa in the mid-troposphere, were similar to the locations air parcel dehydration identified in the upper troposphere by *Dessler and Minschwaner* [2007].

4.2.Asian Monsoon region

The Asian Monsoon region has the world's "most complex patterns of spatial and temporal distribution of stable isotope composition of precipitation" [*Araguas-Araguas et al.*, 1998]. Over mainland Southeast Asia, southern China and the southern Tibetan Plateau, precipitation $\delta^{18}O$ is more depleted during summer than winter, opposite the region's temperature seasonality, and the isotope seasonality across the rest of the northern hemisphere. Under sufficiently strong monsoon conditions, this pattern can extend as far as the North China Plain [*Yamanaka et al.*, 2004], eastern Mongolia [*Sato et al.*, 2007] and the western Tibetan plateau [*Tian et al.*, 2007]. Further north, the regular seasonality resumes, with more depleted winter and less depleted summer precipitation $\delta^{18}O$ [*Yamanaka et al.*, 2007; *Yu et al.*, 2007]. The transition between these two regions is thought represent the transition between the influence of the monsoon and mid-latitude westerlies [*Araguas-Araguas et al.*, 1998; *Tian et al.*, 2001; *Johnson and Ingram*, 2004; *Tian et al.*, 2007; *Peng et al.*, 2010].

In GCMs, the reverse seasonality across the southern region was seen at Hong Kong in ECHAM simulations [*Hoffmann and Heimann*, 1997] and in the global analyses of *Noone and Simmonds* [2002] and *Brown et al.* [2006]. Interannually, *Vuille et al.* [2005] found, through a detailed diagnosis of monsoon circulation over the Indian Ocean, that the JJA precipitation $\delta^{18}O$ depletion increased with the strength of the monsoon circulation, which was attributed to stronger upstream convection and rainout.

This reverse seasonality is typical of low-latitudes where the wet-season is warmer than the dry season, but is most pronounced and has been examined in the most detail over the Asian Monsoon region, and was considered specifically in terms of the seasonal contribution of PCE. For CTRL, the reverse seasonality is present (Figure 11), with a mean DJF-JJA difference of 5.9‰ in the southeast (SE) China domain, compared to –6.2‰ in the northwest (NW) China domain (Table 2), which are within the range of differences observed from GNIP data by *Araguas-Araguas et al.* [1998]. We note that this seasonality was not apparent over land in simulations using the initial isotopically-equipped version of the GISS model [*Jouzel et al.*, 1987], reflecting continual improvements in model resolution and cloud physics parameterization. For INIT, the precipitation seasonality is largely absent across the SE China domain, with a DJF-JJA difference of only 0.6‰. That is, we can attribute this region's reverse isotopic seasonality to PCE, associated with vigorous atmospheric moisture recycling in the intensive convection regions upstream, that depletes the vapor reservoir from which Asian Monsoon precipitation falls. Over the NW China domain, by contrast, the absence of PCE for INIT had a much smaller effect, still with a DJF-JJA difference of -5.6‰, reflecting a weak monsoon influence over that region.

The unique isotopic features of the Asian monsoon region were examined for vapor δD from TES by *Brown et al.* [2008]. The instantaneous observations from their Asian Monsoon study region (15-30^{o}N, 80-100^{o}E) are shown in Figure 12 along with the monthly mean GCM data for the CTRL and INIT experiments over the same region. The comparison of the mean GCM profiles to these instantaneous observations is imperfect, but illustrates how the absence of PCE can explain the extra-Rayleigh branch of their measurements. During the dry DJF season, there is a tendency towards more depleted δD with decreasing q in the TES δD. In *Brown et al.* [2008] the DJF observations were well-predicted by simple atmospheric mixing and idealized Rayleigh distillation, both similar to those used in *Worden et al.* [2007]. This was not the case during the JJA monsoon season, where the moist observations fell below the Rayleigh curves, and in fact exhibited a weak tendency towards more depleted δD with increasing q. *Brown et al.* [2008] proposed that this extra-Rayleigh depletion was the result of upstream atmospheric moisture recycling. We note also that *Herbin et al.* [2009] observed similar extra-Rayleigh depletion using satellite-based vapor δD measurements of a single major typhoon event in 2007 due east of *Brown et al.* [2008]'s Asian Monsoon study region.

For the CTRL run during DJF, the modeled q-δD distribution is Rayleigh-like, with sharply depleting δD with decreasing q, consistent with the analytical model constraints of the observations in *Brown et al.* [2008]. The GCM values are less humid than the TES measurements, but with excellent agreement in the isotopic composition. During JJA, there is an opposite distribution, where δD decreases with increasing q. While this distribution is consistent with TES observations, the extra-Rayleigh depletion is more pronounced, and could indicate excessive atmospheric vapor recycling in the GCM. During DJF in the INIT simulation, the q-δD values have a similar distribution as CTRL, but the mean δD is 32‰ less depleted than CTRL, indicating some contribution from PCE. During the wet JJA, however, the δD was 81‰ less depleted, and with no extra-Rayleigh branch. Furthermore, across the pan-tropical domain of *Worden et al.* [2007], an extra-Rayleigh branch was present for CTRL, but absent for INIT (not shown). This indicates that atmospheric moisture recycling indeed has a generally important role in isotopic depletion of vapor.

4.3.Dry tropics/subtropics

At low latitudes, the largest precipitation $\delta^{18}O$ decrease of ~8‰ for INIT occurred over the dry-subtropics (Figure 5), representing an enriching effect of PCE on precipitation $\delta^{18}O$. This can be explained by the strong equilibration between the light, small-radius droplets falling through the humid and relatively un-depleted surface layer, as has been previously suggested [*Lee et al.*, 2007; *Lee and Fung*, 2008]. Conversely, one can see that PCE has less effect on the vapor $\delta^{18}O$ at the surface (Figure 6); although the PCE has a strong enriching effect on the precipitation that does occur, precipitation is too sparse to have a substantive depleting effect on the $\delta^{18}O$ composition of the ambient vapor compared to the wet tropics.

The subtropical changes to vapor without PCE can also be compared with *Galewsky et al.*'s [2007] vapor δD measurements over Hawaii for late July 2006, which represent an intermediate regime between the wet and dry tropics. In that study, in-situ vapor measurements of δD were taken between sea-level and 4000m, and interpreted using a model (MATCH) with realistic moisture transport, condensation and isotopic fractionation, but which excluded detailed microphysical processes such as condensate re-evaporation. The model predictions spanned the observations, but with the model also tending toward less depleted values. Figure 10 shows mean modeled q and δD distributions over the Hawaii region for July and August, along with the Mauna Kea observations, and q-δD curves for the GCM experiments here. For CTRL, the GCM tended towards slightly higher vapor δD values, particularly over the transition between the boundary layer and troposphere. This bias, however, increased significantly in the absence of PCE for the INIT run. As with the TES measurements, the comparison of the mean GCM profiles to this limited set of instantaneous observations is imperfect, but the consistency with which the INIT and MATCH models produce more under-depleted vapor does qualitatively support the contribution of PCE to vapor depletion.

There were also signatures of PCE in the dry, subtropical anticyclones downstream from the continental convective regions during DJF over the Amazon and southern Africa discussed in the previous section (Figure 6). The air detrained from the mid-tropospheric convective outflow is relatively moist, but heavily depleted, and, by mass, therefore has a substantial isotopic signature when detrained into the dry air. The total contribution of continental, convective outflow to the subtropical moisture is not well-constrained, but has been identified as one of three major atmospheric contributors to moisture in these regions, along with equatorward return flow and subsidence [*Pierrehumbert*, 1998]. Furthermore, contributions of upstream atmospheric moisture recycling in dry tropical conditions have been described in the mesoscale. *Lawrence et al.* [2004] observed highly depleted vapor ^{18}O downwind of organized convection in a high temporal-resolution in-situ sampling downwind of individual storm events, suggesting the depletion provided strong evidence for atmospheric moisture recycling within the storms.

4.4.Extratropics

Strong seasonal effects of PCE were seen in the extra-tropics, and were strongly influenced by the transition to snow-dominated precipitation. During DJF, there was an average increase of ~5‰ in precipitation $\delta^{18}O$ over NH land for INIT compared to CTRL (Figure 5). Spatially, the increase was relatively constant compared to the strong depletion towards the continental interiors for CTRL, which can be attributed to Rayleigh depletion. As the snow line moved northward during JJA, so did the transition from net decrease to net increase in precipitation $\delta^{18}O$ for INIT. Another contributing factor to the seasonal changes in effects of PCE is evapotranspiration from the land surface.

Precipitation $\delta^{18}O$ for INIT undergoes a net decrease over much of North America and Eurasia during JJA when plant transpiration is active, but not during DJF (Figure 5).

Over Eurasia, up to 5‰ of the DJF precipitation $\delta^{18}O$ depletion was attributed to PCE (Figure 5), in addition to that from Rayleigh depletion. *Kurita et al.* [2004], however, found good agreement between a strict Rayleigh-based model of isotopic depletion similar to Eq. 1, with no significant under-depletion despite the model's lack of PCE. This can be explained by the fact that their model was initialized with observed isotopic values in western Russia where DJF precipitation predominantly occurs as snow [*Dai*, 2001]. That is, their initial values from observations were within the snowline and would have reflected any depletion that resulted from PCE from upstream liquid precipitation, over the Atlantic Ocean from which the moisture ultimately originates [*Kurita et al.*, 2004].

Sodemann et al. [2008] recently analyzed NAO controls on Greenland precipitation $\delta^{18}O$ using a trajectory-based model accounting for mixed-phase precipitation, but not PCE. They identified strong NAO controls on the precipitation $\delta^{18}O$, but also found that modeled values were 13-14‰ under-depleted relative to observations from ice core data in southern central Greenland, which ranged from -35 to -38‰ during the winter months. They attributed the under-depletion to possible factors such as the delayed onset of condensation along a trajectory and insufficient orographic distillation. For CTRL, the GCM mean precipitation $\delta^{18}O$ during DJF of – 37‰ accurately captured the observed values. For INIT, the DJF precipitation $\delta^{18}O$ over their site was 7‰ less depleted, and so half of their under-depletion could possibly be explained by the absence of PCE in their model. During JJA, there was an increase in the INIT difference to 13‰ , which can be explained by the northward shift in the snowline. There is an increase in the amount of nearby upstream precipitation which has occurred as liquid, but the precipitation over the Greenland interior still occurs as snow. This increased upstream liquid precipitation results in greater PCE depletion of the vapor reservoir, with no local PCE enrichment.

5. Temperature effect

The most important isotopic phenomenon in the extra-tropics is the positive relationship between precipitation $\delta^{18}O$ and temperature [*Dansgaard*, 1964]. The local, temporal, correlation between temperature and precipitation $\delta^{18}O$ was first modeled by *Hoffman et al.* [1998], and subsequently over specific regions and using various isotopically-equipped GCMs [*Cole et al.*, 1999; *Noone and Simmonds*, 2002; *Vuille and Werner*, 2005; *Schmidt et al.*, 2007; *Risi et al.*, 2010b].

Figure 13 shows the local correlation between monthly anomalies (seasonal cycle removed) of surface temperature (T) and precipitation $\delta^{18}O$ for all months of the year, to quantify the temperature effect at the inter-annual scale, similar to many previous GCM studies. Only correlations with $|r| > 0.2$ and significant at the 95% level are plotted. There is a positive temperature correlation over extra-tropical land, and over some regions of equatorial South America and Africa. We note first that the extra-tropical correlations between temperature and precipitation $\delta^{18}O$ anomalies during all months of the year in Figure 13, and in previous studies, can be viewed as the combination of a strong winter correlation and a weak summer correlation (Figure 14). This difference has not been identified in GCM studies for the extra-tropics, but has been in observational studies. Using observations pooled across Russia, for example, *Kurita et al.* [2004] identified an inter-annual temperature-precipitation $\delta^{18}O$ correlation of r = 0.48 during DJF, which decreased to r = 0.26 during JJA.

The INIT experiment provides an additional mechanistic, and perhaps surprising, partitioning of the temperature effect during DJF. Over much of the extra-tropical NH, the temperature effect was unaffected by the absence of PCE (Figure 14). In these regions, the Rayleigh-distillation interpretation of the temperature effect would apply. For a time-series averaged over central Russia (50°-60°N, 75°-95°E) for example, the DJF T-$\delta^{18}O$ anomaly correlation was r = 0.74 for both CTRL and INIT, consistent with *Kurita et al.'s* [2004] attribution of T-$\delta^{18}O$ anomaly correlations to Rayleigh depletion for seasons other than JJA. There was a slight decrease in the $\delta^{18}O$/T slope from 0.40 ‰/C for CTRL to 0.31 ‰/C for INIT.

Over the US and Europe, however, none of the temperature effect could be attributed to Rayleigh depletion. Over central Europe (45°-55°N, 5°-20°E) the DJF T-$\delta^{18}O$ anomaly correlation was r = 0.55 for CTRL, consistent with the positive local correlations from previous studies [*Rozanski et al.*, 1992; *Baldini et al.*, 2008; *Field*, 2010]. For INIT, by contrast, the DJF correlation reduced to a weak, and negative, r = -0.27. Similarly, the $\delta^{18}O$/T slope decreased from 0.34 ‰/C for CTRL to -0.08 ‰/C for INIT.

We suggest that over these regions during DJF, the temperature effect is attributable to PCE, rather than Rayleigh depletion. The physical mechanism can be understood by noticing that the regions where the temperature effect is absent for INIT correspond to transition between liquid and solid-phase precipitation which separated regions of net increase and net decrease in precipitation $\delta^{18}O$ for INIT (Figure 5). Warmer temperatures are associated with an increase in the proportion of precipitation falling as rainfall, which is locally enriched through PCE and will have higher $\delta^{18}O$ values. Colder temperatures are associated with more precipitation falling as snow, which will not be locally enriched through PCE and have lower $\delta^{18}O$ values. That is, temperature controls the phase of precipitation, which controls whether or not local enrichment through PCE occurs. This control exists only in regions where there is variability in the proportion of precipitation which falls as snow.

Curiously, there was also the emergence of a band of significant negative T-$\delta^{18}O$ correlation for INIT, particularly over the Southern Ocean (Figure 14). That is, in the absence of PCE with highly un-depleted surface evaporate, pure Rayleigh depletion results in a negative temperature effect. This is because the fractionation factor (α in Eq. 1) for vapor to ice deposition is greater than that for vapor to liquid [*Majoube*, 1971a; b]. As a precipitating air mass transitions from rainfall to snowfall, the precipitation $\delta^{18}O$ in fact undergoes a ~2‰ enrichment simply due to this transition in phase. This acts as a discrete, step-wise, and positive influence over the $\delta^{18}O$ value of condensate in the transition zone from rain to snow, incurred simply via the temperature-controlled transition to snowfall. For CTRL, where PCE is present, this effect is masked by the opposite depleting effect of the lack of PCE enrichment during snowfall.

Given the importance of the transition from rain to snowfall-dominated precipitation, we conducted follow-up diagnoses to determine the extent to which $\delta^{18}O$ variability could be explained, more directly, by the phase of precipitation. Figure 15 shows the DJF correlation between precipitation $\delta^{18}O$ and the fraction of snow falling as precipitation. For CTRL, there is indeed a strong negative correlation between the proportion of precipitation falling as snow and precipitation $\delta^{18}O$; higher snow fraction is associated with less enrichment from PCE and, as a result, more depleted $\delta^{18}O$. For INIT, this effect is absent, and regions of positive correlation emerge, which are associated with the higher fractionation factor for the vapor-snow change of phase relative to the vapor-liquid change of phase.

Thus, the broad extra-tropical bands of positive temperature correlation seen during DJF in Figure 14 are in fact the superposition of two correlation patterns with distinct underlying mechanisms: Rayleigh depletion, and PCE. The European case is interesting because of the availability of high-quality precipitation $\delta^{18}O$ data from the GNIP network, which has resulted in a succession of studies over the region, starting with *Sonntag and Schoch-Fischer* [1985] and *Rozanski et al.* [1992]. Recently, *Baldini et al.* [2008] and *Field* [2010] examined the controls over European $\delta^{18}O$, identifying regional temperature and the underlying atmospheric circulation controls in the form of the North Atlantic Oscillation and Northern Annular Mode as important. Implicit in these studies was an assumption that the observed temperature effect was the result of Rayleigh depletion; less-depleted $\delta^{18}O$ was associated with less upstream Rayleigh depletion, which was in turn influenced by characteristic patterns of atmospheric circulation. The results of the INIT experiment suggest an alternative mechanism: during DJF the temperature effect is governed by variability of precipitation falling as rain or snow, via the occurrence or not of PCE.

6. Conclusions

In this study, we have quantified the effects of post-condensation exchange on the isotopic composition of precipitation and vapor using a GCM. PCE is widely acknowledged as an important influence on precipitation $\delta^{18}O$, but this study offers quantified, regional contributions of PCE on a global scale.

The key findings were:

1. PCE tends to deplete the heavy isotopes of water vapor, as was seen in *Wright et al.* [2009], on the order of 10-15‰ in regions of intense tropical atmospheric moisture recycling or in the warm extratropics.
2. At low latitudes, PCE tends to enrich local precipitation $\delta^{18}O$ via exchange with fresh, relatively un-depleted surface evaporate by up to ~8 ‰ in regions of light precipitation. However, this local enrichment can be offset, or exceeded, by depletion of the precipitation's vapor source, which is associated with intensive atmospheric moisture recycling in the convective column, following *Risi et al.* [2008]. At high latitudes, local precipitation enrichment can be exceeded by upstream depletion of the vapor reservoir.

3. The low and high latitude regimes are separated by the transition from rain to snow-dominated precipitation. Precipitation falling as snow is subject to upstream isotopic depletion via PCE, but undergoes no local enrichment. The greatest PCE depletion of ~13 ‰ was seen over Greenland during JJA, with values roughly half of those found in the North American and Eurasian continental interiors during DJF.
4. The reverse isotopic seasonality observed in the Asian Monsoon region can be attributed to PCE, presumably via intensive upstream moisture recycling. The suggestion that extra-Rayleigh depletion seen in the TES δD observations in *Worden et al.* [2007] and *Brown et al.* [2008] is the result of upstream moisture recycling is supported by the GCM experiments.
5. The cold-season temperature effect is the superposition of Rayleigh-depletion where it snows, and PCE where precipitation falls as a mix of rain and snow.

The experiments conducted in this analysis illustrate a potential approach for future interpretation studies of vapor isotope measurements, which are considered an exciting new means through which to understand moist processes in the atmosphere [*Sherwood et al.*, 2010]. Along with in-situ measurements for specific regions, it would also be useful to compare these results with other satellite-based measurements of the isotopic composition of vapor [*Frankenberg et al.*, 2009; *Herbin et al.*, 2009]. Important for future studies of satellite-based measurements would be an examination of the effect of averaging kernel smoothing in the retrievals, and differences between clear and cloudy-sky retrievals.

There remains much investigation to be done along these lines with isotopically-equipped GCMs. Indeed, this study was comprised of a single, global-scale GCM experiment, describing the effects of PCE from the tropics to the poles. It would be interesting in the future to conduct more detailed mechanistic studies for specific regions, partitioning, for example, the effects of condensate re-evaporation from equilibration at low latitudes, as distinguished by *Risi et al.* [2008], or the effects of equilibrium and kinetic deposition to ice in cold regions. It would also be useful to conduct such studies across additional isotopically-equipped GCMs, to determine the sensitivity to particular cloud and isotope physics parameterizations, particularly for GCMs which have recently been equipped with more sophisticated post-condensation exchange schemes [*Yoshimura et al.*, 2008; *Risi et al.*, 2010b]. Given the importance of the phase of precipitation, it would also be worth revisiting observational GNIP data for Europe, where the data density is high, and for which this study showed a strong contribution of PCE through its relationship with mixed phase precipitation.

Acknowledgements

The authors thank Joe Galewsky for the vapor δD measurements over Mauna Kea, John Worden for helpful comments, and Gavin Schmidt for guidance in using ModelE. This work was supported by the Canadian Foundation for Climate and Atmospheric Sciences through the Polar Climate Stability Network, and for RF by a graduate scholarship from the Natural Sciences and Engineering Research Council of Canada.

References

Aldaz, L., and S. Deutsch (1967), On a Relationship Between Air Temperature and Oxygen Isotope Ratio of Snow and Firn in South Pole Region, *Earth and Planetary Science Letters*, *3*(3), 267-274.

Araguas-Araguas, L., K. Froehlich, and K. Rozanski (1998), Stable Isotope Composition of Precipitation Over Southeast Asia, *Journal of Geophysical Research-Atmospheres*, *103*(D22), 28721-28742.

Bacmeister, J. T., M. J. Suarez, and F. R. Robertson (2006), Rain reevaporation, boundary layer-convection interactions, and Pacific rainfall patterns in an AGCM, *Journal of the Atmospheric Sciences*, *63*(12), 3383-3403.

Baldini, L. M., F. McDermott, A. M. Foley, and J. U. L. Baldini (2008), Spatial variability in the European winter precipitation delta O-18-NAO relationship: Implications for reconstructing NAO-mode climate variability in the Holocene, *Geophysical Research Letters*, *35*(4), L04709, doi:10.1029/2007gl032027.

Beer, R., T. A. Glavich, and D. M. Rider (2001), Tropospheric emission spectrometer for the Earth Observing System's Aura Satellite, *Applied Optics*, *40*(15), 2356-2367.

Brown, D., J. Worden, and D. Noone (2008), Comparison of atmospheric hydrology over convective continental regions using water vapor isotope measurements from space, *Journal of Geophysical Research-Atmospheres*, *113*(D15), D15124,doi :10.1029/2007jd009676.

Brown, J., I. Simmonds, and D. Noone (2006), Modeling delta O-18 in tropical precipitation and the surface ocean for present-day climate, *Journal of Geophysical Research-Atmospheres*, *111*(D5), Artn D05105, Doi 10.1029/2004jd005611.

Celle-Jeanton, H., R. Gonfiantini, Y. Travi, and B. Sol (2004), Oxygen-18 Variations of Rainwater During Precipitation: Application of the Rayleigh Model to Selected Rainfalls in Southern France, *Journal of Hydrology*, *289*(1-4), 165-177.

Ciais, P., and J. Jouzel (1994), Deuterium and Oxygen-18 in Precipitation - Isotopic Model, Including Mixed Cloud Processes, *Journal of Geophysical Research-Atmospheres*, *99*(D8), 16793-16803.

Cole, J. E., D. Rind, R. S. Webb, J. Jouzel, and R. Healy (1999), Climatic Controls on Interannual Variability of Precipitation Delta O-18: Simulated Influence of Temperature, Precipitation Amount, and Vapor Source Region, *Journal of Geophysical Research-Atmospheres*, *104*(D12), 14223-14235.

Dai, A. (2001), Global precipitation and thunderstorm frequencies. Part I: Seasonal and interannual variations, *Journal of Climate*, *14*(6), 1092-1111.

Danis, P. A., V. Masson-Delmotte, M. Stievenard, M. T. Guillemim, V. Daux, P. Naveau, and U. von Grafenstein (2006), Reconstruction of past precipitation beta O-18 using tree-ring cellulose delta O-18 and delta C-13: A calibration study near Lac d'Annecy, France, *Earth and Planetary Science Letters*, *243*(3-4), 439-448, 10.1016/j.epsl.2006.01.023.

Dansgaard, W. (1954), The O-18-Abundance in Fresh Water, *Geochimica Et Cosmochimica Acta*, *6*(5-6), 241-260.

Dansgaard, W. (1964), Stable Isotopes in Precipitation, *Tellus*, *16*(4), 436-468.

Dessler, A. E., and K. Minschwaner (2007), An analysis of the regulation of tropical tropospheric water vapor, *Journal of Geophysical Research-Atmospheres*, *112*(D10), Artn D10120, Doi 10.1029/2006jd007683.

Ekaykin, A. A. (2003), Meteorological regime of central Antarctica and its role in the formation of isotope composition of snow thickness, 122pp pp, University Joseph Fourier, Grenoble, France.

Etien, N., V. Daux, V. Masson-Delmotte, M. Stievenard, V. Bernard, S. Durost, M. T. Guillemin, O. Mestre, and M. Pierre (2008), A bi-proxy reconstruction of Fontainebleau (France) growing season temperature from AD 1596 to 2000, *Climate of the Past*, *4*(2), 91-106.

Feng, X. H., A. M. Faiia, and E. S. Posmentier (2009), Seasonality of isotopes in precipitation: A global perspective, *Journal of Geophysical Research-Atmospheres*, *114*, D08116, doi:10.1029/2008jd011279.

Field, R. D. (2010), Observed and modeled controls on precipitation δ18O over Europe: from local temperature to the Northern Annular Mode, *Journal of Geophysical Research-Atmospheres*, *115*(D12101), doi:10.1029/2009JD013370.

Frankenberg, C., K. Yoshimura, T. Warneke, I. Aben, A. Butz, N. Deutscher, D. Griffith, F. Hase, J. Notholt, M. Schneider, H. Schrijver, and T. Rockmann (2009), Dynamic Processes Governing Lower-Tropospheric HDO/H2O Ratios as Observed from Space and Ground, *Science*, *325*(5946), 1374-1377, DOI 10.1126/science.1173791.

Friedman, I., L. Machta, and R. Soller (1962), Water-Vapor Exchange between a Water Droplet and Its Environment, *Journal of Geophysical Research*, *67*(7), 2761-2766.

Friedman, I., J. M. Harris, G. I. Smith, and C. A. Johnson (2002), Stable isotope composition of waters in the Great Basin, United States - 1. Air-mass trajectories, *Journal of Geophysical Research-Atmospheres*, *107*(D19), 4400, doi: 10.1029/2001jd000565.

Galewsky, J., M. Strong, and Z. D. Sharp (2007), Measurements of water vapor D/H ratios from Mauna Kea, Hawaii, and implications for subtropical humidity dynamics, *Geophysical Research Letters*, *34*(22), L22808,:10.1029/2007gl031330.

Gat, J. R., and E. Matsui (1991), Atmospheric Water-Balance in the Amazon Basin - an Isotopic Evapotranspiration Model, *Journal of Geophysical Research-Atmospheres*, *96*(D7), 13179-13188.

Gat, J. R. (2000), Atmospheric Water Balance - the Isotopic Perspective, *Hydrological Processes*, *14*(8), 1357-1369.

Gedzelman, S. D., and R. Arnold (1994), Modeling the Isotopic Composition of Precipitation, *Journal of Geophysical Research-Atmospheres*, *99*(D5), 10455-10471.

Gonfiantini, R., M. A. Roche, J. C. Olivry, J. C. Fontes, and G. M. Zuppi (2001), The Altitude Effect on the Isotopic Composition of Tropical Rains, *Chemical Geology*, *181*(1-4), 147-167.

Hastings, M. G., E. J. Steig, and D. M. Sigman (2004), Seasonal variations in N and O isotopes of nitrate in snow at Summit, Greenland: Implications for the study of nitrate in snow and ice cores, *Journal of Geophysical Research-Atmospheres*, *109*(D20), Artn D20306, Doi 10.1029/2004jd004991.

Helsen, M. M., R. S. W. Van De Wal, and M. R. Van Den Broeke (2007), The Isotopic Composition of Present-Day Antarctic Snow in a Lagrangian Atmospheric Simulation, *Journal of Climate*, *20*(4), 739-756.

Herbin, H., D. Hurtmans, C. Clerbaux, L. Clarisse, and P. F. Coheur (2009), (H2O)-O-16 and HDO measurements with IASI/MetOp, *Atmospheric Chemistry and Physics*, *9*(24), 9433-9447.

Hoffmann, G., and M. Heimann (1997), Water Isotope Modeling in the Asian Monsoon Region, *Quaternary International*, *37*, 115-128.

Hoffmann, G., M. Werner, and M. Heimann (1998), Water Isotope Module of the ECHAM Atmospheric General Circulation Model: a Study on Timescales From Days to Several Years, *Journal of Geophysical Research-Atmospheres*, *103*(D14), 16871-16896.

IAEA (2001), GNIP Maps and animations, edited, International Atomic Energy Agency, Vienna.

Johnson, K. R., and B. L. Ingram (2004), Spatial and Temporal Variability in the Stable Isotope Systematics of Modern Precipitation in China: Implications for Paleoclimate Reconstructions, *Earth and Planetary Science Letters*, *220*(3-4), 365-377.

Jouzel, J., G. L. Russell, R. J. Suozzo, R. D. Koster, J. W. C. White, and W. S. Broecker (1987), Simulations of the HDO and H2 O-18 Atmospheric Cycles Using the NASA GISS General-Circulation Model - the Seasonal Cycle for Present-Day Conditions, *Journal of Geophysical Research-Atmospheres*, *92*(D12), 14739-14760.

Jouzel, J., R. B. Alley, K. M. Cuffey, W. Dansgaard, P. Grootes, G. Hoffmann, S. J. Johnsen, R. D. Koster, D. Peel, C. A. Shuman, M. Stievenard, M. Stuiver, and J. White (1997), Validity of the Temperature Reconstruction From Water Isotopes in Ice Cores, *Journal of Geophysical Research-Oceans*, *102*(C12), 26471-26487.

Kavanaugh, J. L., and K. M. Cuffey (2003), Space and time variation of delta O-18 and delta D in Antarctic precipitation revisited, *Global Biogeochemical Cycles*, *17*(1), Artn 1017, Doi 10.1029/2002gb001910.

Kurita, N., N. Yoshida, G. Inoue, and E. A. Chayanova (2004), Modern isotope climatology of Russia: A first assessment, *Journal of Geophysical Research-Atmospheres*, *109*(D3), 15, D03102, doi:10.1029/2003jd003404.

Lawrence, J. R., S. D. Gedzelman, D. Dexheimer, H. K. Cho, G. D. Carrie, R. Gasparini, C. R. Anderson, K. P. Bowman, and M. I. Biggerstaff (2004), Stable isotopic composition of water vapor in the tropics, *Journal of Geophysical Research-Atmospheres*, *109*(D6), Artn D06115, Doi 10.1029/2003jd004046.

Lee, J. E., I. Fung, D. J. DePaolo, and C. C. Henning (2007), Analysis of the global distribution of water isotopes using the NCAR atmospheric general circulation model, *Journal of Geophysical Research-Atmospheres*, *112*(D16), D16306, doi: 10.1029/2006jd007657.

Lee, J. E., and I. Fung (2008), "Amount effect" of water isotopes and quantitative analysis of post-condensation processes, *Hydrological Processes*, *22*(1), 1-8, Doi 10.1002/Hyp.6637.

Majoube, M. (1971a), Oxygen-18 and Deuterium Fractionation Between Water and Steam, *Journal De Chimie Physique Et De Physico-Chimie Biologique*, *68*(10), 1423-1436.

Majoube, M. (1971b), Fractionation in O-18 Between Ice and Water Vapor, *Journal De Chimie Physique Et De Physico-Chimie Biologique*, *68*(4), 625-636.

Maloney, E. D. (2009), The Moist Static Energy Budget of a Composite Tropical Intraseasonal Oscillation in a Climate Model, *Journal of Climate*, *22*(3), 711-729, doi: 10.1175/2008jcli2542.1.

Masson-Delmotte, V., S. Hou, A. Ekaykin, J. Jouzel, A. Aristarain, R. T. Bernardo, D. Bromwich, O. Cattani, M. Delmotte, S. Falourd, M. Frezzotti, H. Gallee, L. Genoni, E. Isaksson, A. Landais, M. M. Helsen, G. Hoffmann, J. Lopez, V. Morgan, H. Motoyama, D. Noone, H. Oerter, J. R. Petit, A. Royer, R. Uemura, G. A. Schmidt, E. Schlosser, J. C. Simoes, E. J. Steig, B. Stenni, M. Stievenard, M. R. van den Broeke, R. S. W. V. de Wal, W. J. V. de Berg, F. Vimeux, and J. W. C. White (2008), A review of Antarctic surface snow isotopic composition: Observations, atmospheric circulation, and isotopic modeling, *Journal of Climate*, *21*(13), 3359-3387, Doi 10.1175/2007jcli2139.1.

Noone, D., and I. Simmonds (2002), Associations Between Delta O-18 of Water and Climate Parameters in a Simulation of Atmospheric Circulation for 1979-95, *Journal of Climate*, *15*(22), 3150-3169.

Noone, D., and C. Sturm (2010), Comprehensive Dynamical Models of Global and Regional Water Isotope Distributions, in *Isoscapes: Understanding Movement, Pattern and Process on Earth Through Isotope Mapping*, edited by J. B. West, et al., pp. 195-219, Springer, Dordrecht.

Peng, T. R., C. H. Wang, C. C. Huang, L. Y. Fei, C. T. A. Chen, and J. L. Hwong (2010), Stable isotopic characteristic of Taiwan's precipitation: A case study of western Pacific monsoon region, *Earth and Planetary Science Letters*, *289*(3-4), 357-366, DOI 10.1016/j.epsl.2009.11.024.

Pierrehumbert, R. T. (1998), Lateral mixing as a source of subtropical water vapor, *Geophysical Research Letters*, *25*(2), 151-154.

Rayner, N. A., D. E. Parker, E. B. Horton, C. K. Folland, L. V. Alexander, D. P. Rowell, E. C. Kent, and A. Kaplan (2003), Global analyses of sea surface temperature, sea ice, and night marine air temperature since the late nineteenth century, *Journal of Geophysical Research-Atmospheres*, *108*(D14), 4407, doi:10.1029/2002jd002670.

Risi, C., S. Bony, and F. Vimeux (2008), Influence of convective processes on the isotopic composition (delta O-18 and delta D) of precipitation and water vapor in the tropics: 2. Physical interpretation of the amount effect, *Journal of Geophysical Research-Atmospheres*, *113*(D19), D19306, doi: 10.1029/2008jd009943.

Risi, C., S. Bony, F. Vimeux, M. Chong, and L. Descroix (2010a), Evolution of the stable water isotopic composition of the rain sampled along Sahelian squall lines, *Quarterly Journal of the Royal Meteorological Society*, *136*, 227-242, Doi 10.1002/Qj.485.

Risi, C., S. Bony, F. Vimeux, and J. Jouzel (2010b), Water stable isotopes in the LMDZ4 General Circulation Model: model evaluation for present day and past climates and applications to climatic interpretations of tropical isotopic records, *J. Geophys. Res.*, doi:10.1029/2009JD013255.

Rozanski, K., C. Sonntag, and K. O. Munnich (1982), Factors Controlling Stable Isotope Composition of European Precipitation, *Tellus*, *34*(2), 142-150.

Rozanski, K., L. Araguas-Araguas, and R. Gonfiantini (1992), Relation Between Long-Term Trends of O-18 Isotope Composition of Precipitation and Climate, *Science*, *258*(5084), 981-985.

Sato, T., M. Tsujimura, T. Yamanaka, H. Iwasaki, A. Sugimoto, M. Sugita, F. Kimura, G. Davaa, and D. Oyunbaatar (2007), Water sources in semiarid northeast Asia as revealed by field observations and isotope transport model, *Journal of Geophysical Research-Atmospheres*, *112*(D17), D17112,:10.1029/2006jd008321.

Schmidt, G. A., G. Hoffmann, D. T. Shindell, and Y. Y. Hu (2005), Modeling Atmospheric Stable Water Isotopes and the Potential for Constraining Cloud Processes and Stratosphere-Troposphere Water Exchange, *Journal of Geophysical Research-Atmospheres*, *110*(D21), D21314, doi: 10.1029/2005jd005790.

Schmidt, G. A., R. Ruedy, J. E. Hansen, I. Aleinov, N. Bell, M. Bauer, S. Bauer, B. Cairns, V. Canuto, Y. Cheng, A. Del Genio, G. Faluvegi, A. D. Friend, T. M. Hall, Y. Y. Hu, M. Kelley, N. Y. Kiang, D. Koch, A. A. Lacis, J. Lerner, K. K. Lo, R. L. Miller, L. Nazarenko, V. Oinas, J. Perlwitz, J. Perlwitz, D. Rind, A. Romanou, G. L. Russell, M. Sato, D. T. Shindell, P. H. Stone, S. Sun, N. Tausnev, D. Thresher, and M. S. Yao (2006), Present-Day Atmospheric Simulations Using GISS ModelE: Comparison to in Situ, Satellite, and Reanalysis Data, *Journal of Climate*, *19*(2), 153-192.

Schmidt, G. A., A. N. LeGrande, and G. Hoffmann (2007), Water isotope expressions of intrinsic and forced variability in a coupled ocean-atmosphere model, *Journal of Geophysical Research-Atmospheres*, *112*(D10), D10103,:10.1029/2006jd007781.

Scholl, M. A., J. B. Shanley, J. P. Zegarra, and T. B. Coplen (2009), The stable isotope amount effect: New insights from NEXRAD echo tops, Luquillo Mountains, Puerto Rico, *Water Resources Research*, *45*, Artn W12407, Doi 10.1029/2008wr007515.

Sherwood, S. C., R. Roca, T. M. Weckwerth, and N. G. Andronova (2010), Tropospheric Water Vapor, Convection, and Climate, *Reviews of Geophysics*, *48*, Artn Rg2001, Doi 10.1029/2009rg000301.

Shuman, C. A., D. H. Bromwich, J. Kipfstuhl, and M. Schwager (2001), Multiyear Accumulation and Temperature History Near the North Greenland Ice Core Project Site, North Central Greenland, *Journal of Geophysical Research-Atmospheres*, *106*(D24), 33853-33866.

Sodemann, H., V. Masson-Delmotte, C. Schwierz, B. M. Vinther, and H. Wernli (2008), Interannual variability of Greenland winter precipitation sources: 2. Effects of North Atlantic Oscillation variability on stable isotopes in precipitation, *Journal of Geophysical Research-Atmospheres*, *113*(D12), D12111,:10.1029/2007jd009416.

Sonntag, C., and H. Schoch-Fischer (1985), Deuterium and Oxygen 18 in Water Vapour and Precipitation: Application to Atmospheric Water Vapour Transport and to Paleoclimate, *Isotopes in Environmental and Health Studies*, *21*(6), 193-198.

Stern, L. A., and P. M. Blisniuk (2002), Stable isotope composition of precipitation across the southern Patagonian Andes, *Journal of Geophysical Research-Atmospheres*, *107*(D23), 4667, doi:10.1029/2002jd002509.

Stewart, M. K. (1975), Stable Isotope Fractionation Due to Evaporation and Isotopic-Exchange of Falling Waterdrops - Applications to Atmospheric Processes and Evaporation of Lakes, *Journal of Geophysical Research*, *80*(9), 1133-1146.

Strong, M., Z. D. Sharp, and D. S. Gutzler (2007), Diagnosing moisture transport using D/H ratios of water vapor, *Geophysical Research Letters*, *34*(3), L03404,doi :10.1029/2006gl028307.

Tian, L., V. Masson-Delmotte, M. Stievenard, T. Yao, and J. Jouzel (2001), Tibetan Plateau Summer Monsoon Northward Extent Revealed by Measurements of Water Stable Isotopes, *Journal of Geophysical Research-Atmospheres*, *106*(D22), 28081-28088.

Tian, L., T. Yao, P. F. Schuster, J. W. C. White, K. Ichiyanagi, E. Pendall, J. Pu, and Y. Wu (2003), Oxygen-18 concentrations in recent precipitation and ice cores on the Tibetan Plateau, *Journal of Geophysical Research-Atmospheres*, *108*(D9), 4293,:10.1029/2002jd002173.

Tian, L. D., T. D. Yao, K. MacClune, J. W. C. White, A. Schilla, B. Vaughn, R. Vachon, and K. Ichiyanagi (2007), Stable isotopic variations in west China: A consideration of moisture sources, *Journal of Geophysical Research-Atmospheres*, *112*(D10), Artn D10112, doi 10.1029/2006jd007718.

van Ommen, T. D., and V. Morgan (1997), Calibrating the ice core paleothermometer using seasonality, *Journal of Geophysical Research-Atmospheres*, *102*(D8), 9351-9357.

Vuille, M., and M. Werner (2005), Stable isotopes in precipitation recording South American summer monsoon and ENSO variability: observations and model results, *Climate Dynamics*, *25*(4), 401-413, doi: 10.1007/s00382-005-0049-9.

Vuille, M., M. Werner, R. S. Bradley, and F. Keimig (2005), Stable isotopes in precipitation in the Asian monsoon region, *Journal of Geophysical Research-Atmospheres*, *110*(D23), D23108, doi: 10.1029/2005jd006022.

Werner, M., and M. Heimann (2002), Modeling interannual variability of water isotopes in Greenland and Antarctica, *Journal of Geophysical Research-Atmospheres*, *107*(D1-D2), 4001, doi: 10.1029/2001jd900253.

Worden, J., K. Bowman, D. Noone, R. Beer, S. Clough, A. Eldering, B. Fisher, A. Goldman, M. Gunson, R. Herman, S. S. Kulawik, M. Lampel, M. Luo, G. Osterman, C. Rinsland, C. Rodgers, S. Sander, M. Shephard, and H. Worden (2006), Tropospheric emission spectrometer observations of the tropospheric HDO/H2O ratio: Estimation approach and characterization, *Journal of Geophysical Research-Atmospheres*, *111*(D16), D16309, doi: 10.1029/2005jd006606.

Worden, J., D. Noone, and K. Bowman (2007), Importance of Rain Evaporation and Continental Convection in the Tropical Water Cycle, *Nature*, *445*(7127), 528-532.

Wright, J. S., A. H. Sobel, and G. A. Schmidt (2009), Influence of condensate evaporation on water vapor and its stable isotopes in a GCM, *Geophysical Research Letters*, *36*, L12804, doi 10.1029/2009gl038091.

Wright, J. S., A. Sobel, and J. Galewsky (in press), Diagnosis of Zonal Mean Relative Humidity Changes in a Warmer Climate, *Journal of Climate*, doi: 10.1175/2010JCLI3488.1.

Yamanaka, T., J. Shimada, Y. Hamada, T. Tanaka, Y. H. Yang, W. J. Zhang, and C. S. Hu (2004), Hydrogen and Oxygen Isotopes in Precipitation in the Northern Part of the North China Plain: Climatology and Inter-Storm Variability, *Hydrological Processes*, *18*(12), 2211-2222.

Yamanaka, T., M. Tsujimura, D. Oyunbaatar, and G. Davaa (2007), Isotopic variation of precipitation over eastern Mongolia and its implication for the atmospheric water cycle, *Journal of Hydrology*, *333*(1), 21-34, doi:10.1016/j.jhydrol.2006.07.022.

Yoshimura, K., T. Oki, N. Ohte, and S. Kanae (2003), A quantitative analysis of short-term O-18 variability with a Rayleigh-type isotope circulation model, *Journal of Geophysical Research-Atmospheres*, *108*(D20), -.

Yoshimura, K., M. Kanamitsu, D. Noone, and T. Oki (2008), Historical isotope simulation using Reanalysis atmospheric data, *Journal of Geophysical Research-Atmospheres*, *113*(D19), D19108, doi:10.1029/2008jd010074.

Yu, W., T. Yao, L. Tian, Y. Ma, N. Kurita, K. Ichiyanagi, Y. Wang, and W. Sun (2007), Stable isotope variations in precipitation and moisture trajectories on the western Tibetan plateau, China, *Arctic Antarctic and Alpine Research*, *39*(4), 688-693.

List of Figures

Figure 10. q-δD profiles over Hawaii for CTRL and INIT, with Mauna Kea observations from *Galewsky et al.* [2007]. Measurements were taken between sea-level and 4000m.

Figure 11. DJF – JJA precipitation $\delta^{18}O$, following *Araguas-Araguas et al.* [1998] and *Vuille et al.* [2005], for CTRL and INIT.

Figure 12. q-δD plots over *Brown et al.'s* [2008] Asian Monsoon region (15-30^{o}N, 80-100^{o}E) for instantaneous TES observations, and mean values from the ModelE CTRL and INIT experiments.

Figure 13. Correlation between monthly surface temperature and precipitation $\delta^{18}O$ anomalies (seasonal cycle removed) for CTRL, during all months of the year.

Figure 14. Correlation between surface temperature and precipitation $\delta^{18}O$ anomalies for the CTRL and INIT experiments, for different seasons. Black contours show the fraction of precipitation falling as snow at the 0.1 and 0.9 levels.

Figure 15. DJF correlation between anomalies of precipitation $\delta^{18}O$ and fraction of precipitation that falls as snow. Black contours show the fraction of precipitation falling as snow at the 0.1 and 0.9 levels.

Tables

Table 1. Correlation (r), bias (b) and root-mean square error (RMSE) for the $\delta^{18}O$ observations and GCM experiments. The statistics across all observations include data for Antarctica, Greenland and Russia to supplement the GNIP data.

		All observations			GNIP only		
		r	**b (‰)**	**RMSE (‰)**	**r**	**b (‰)**	**RMSE (‰)**
DJF	**CTRL**	0.93	-1.0	3.2	0.89	-1.1	3.2
	INIT	0.81	-2.5	5.9	0.65	-2.9	5.8
JJA	**CTRL**	0.92	0.2	3.1	0.72	0.1	2.9
	INIT	0.88	-4.6	6.4	0.37	-5.1	6.2

Table 2. Seasonal changes in precipitation δ^{18}O for SE China (15-30°N, 90-105E) and NW China (30-45N, 75-90°E)

	CTRL			INIT		
	DJF	**JJA**	**DJF-JJA**	**DJF**	**JJA**	**DJF-JJA**
SE China	-7.0	-12.8	5.9	-10.4	-11.0	0.6
NW China	-20.5	-14.3	-6.2	-18.4	-12.8	-5.6

Figures

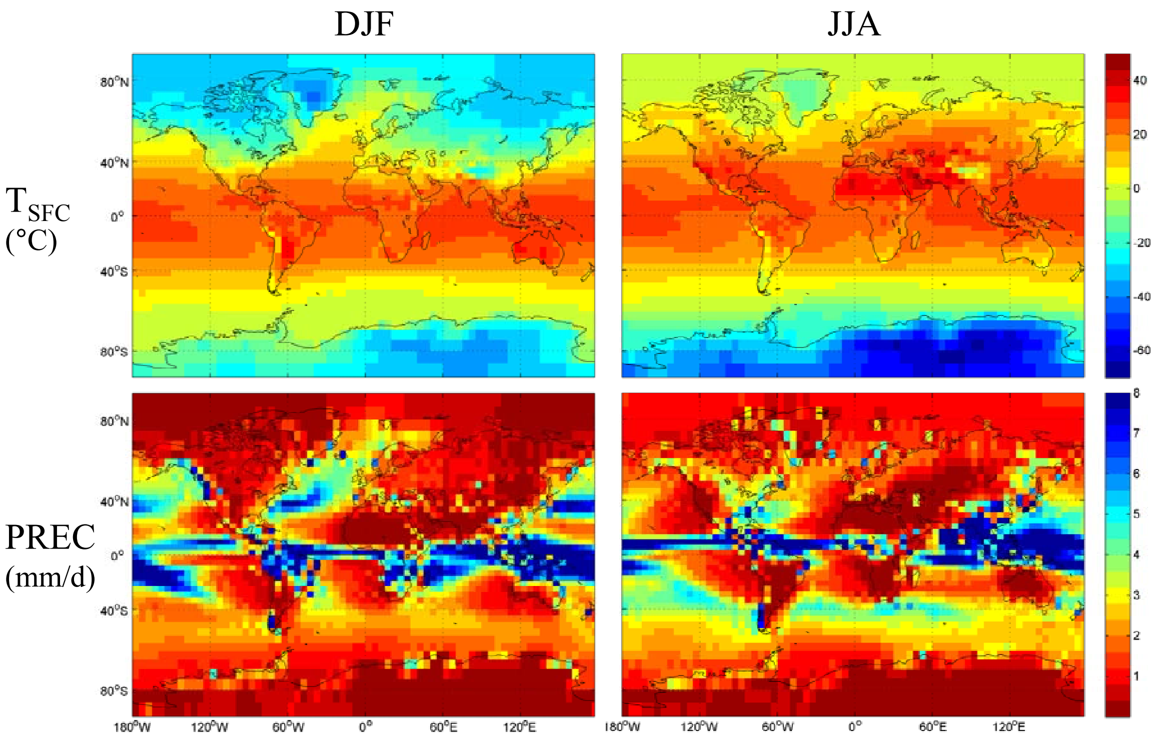

Figure 1. Seasonal surface air temperature and precipitation.

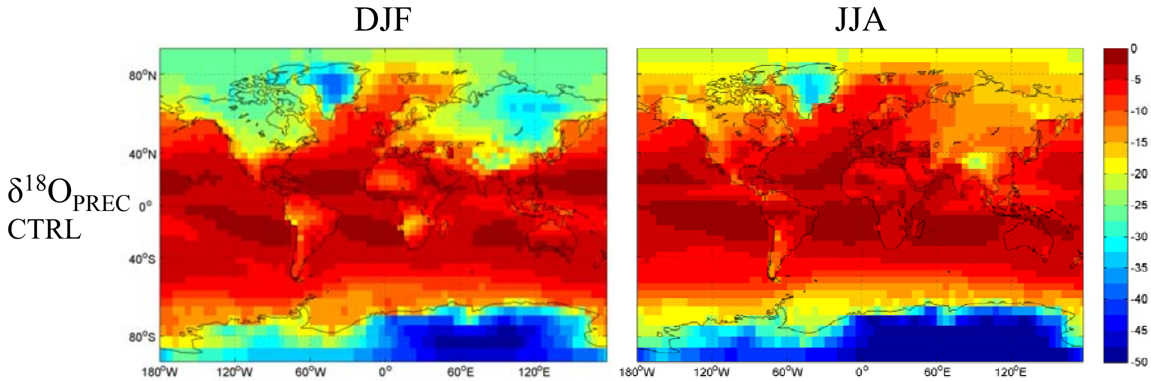

Figure 2. Seasonal $\delta^{18}O$ composition (‰) of precipitation from GISS ModelE CTRL run.

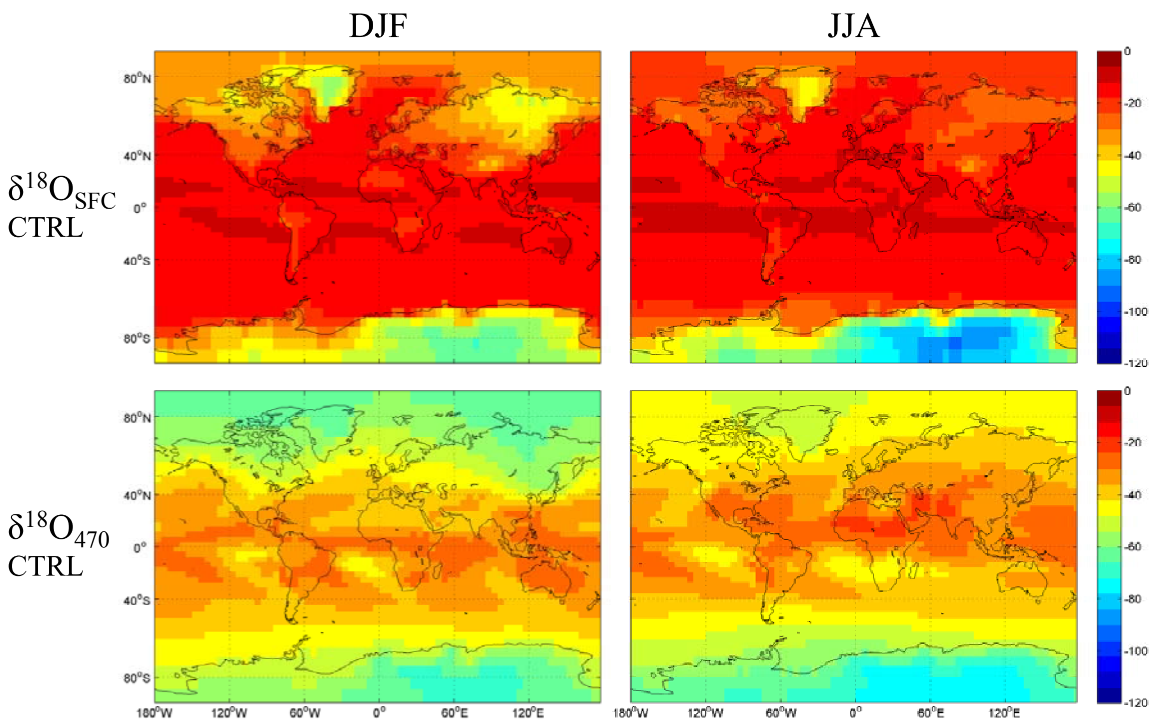

Figure 3. Seasonal $\delta^{18}O$ composition (‰) of surface vapor and vapor at 470 hPa for CTRL.

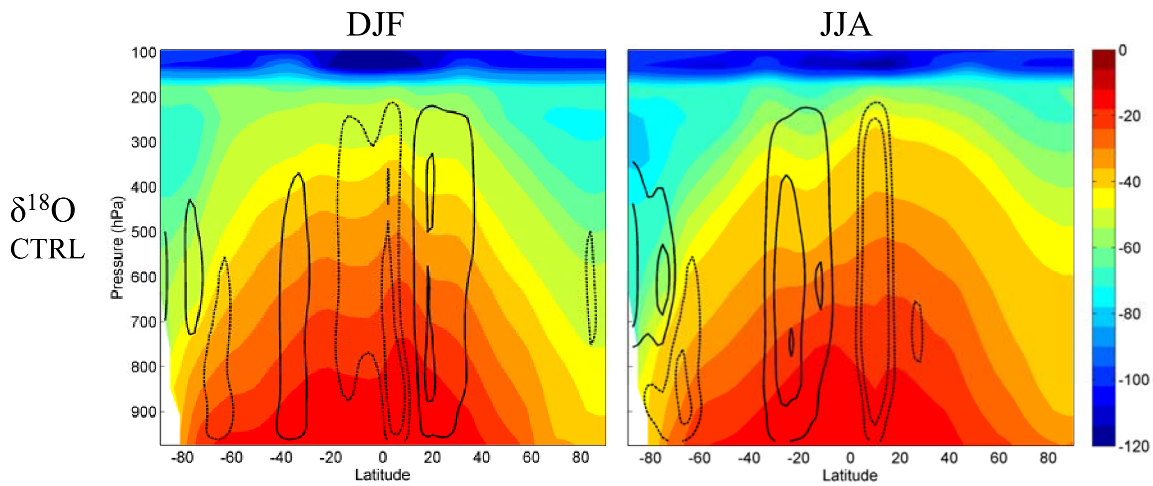

Figure 4. Mean zonal $\delta^{18}O$ of vapor (‰) for CTRL. Contours show vertical velocity ω (10^{-4} hPa/s), with dashed contours for upward motion (ω < 0), and solid contours for downward motion (ω > 0), each at 1 10^{-3} hPa/s contour intervals.

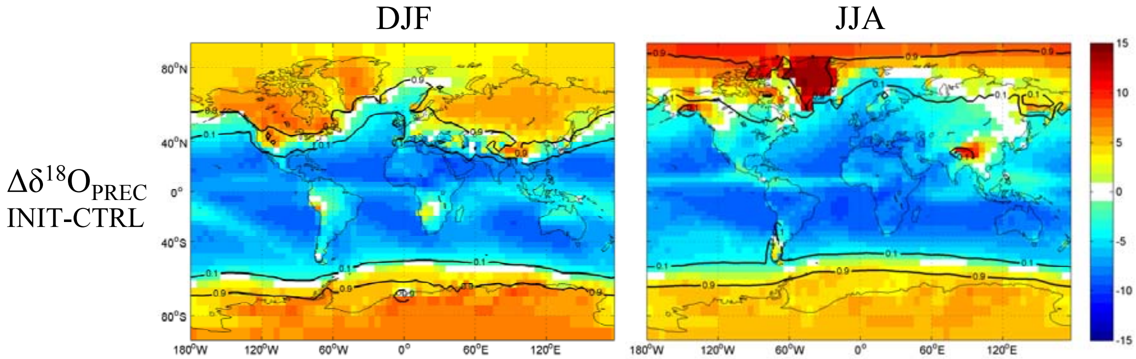

Figure 5. Change in $\delta^{18}O$ composition (‰) for precipitation $\delta^{18}O$ for INIT. Black contours show the fraction of precipitation falling as snow at the 0.1 and 0.9 levels.

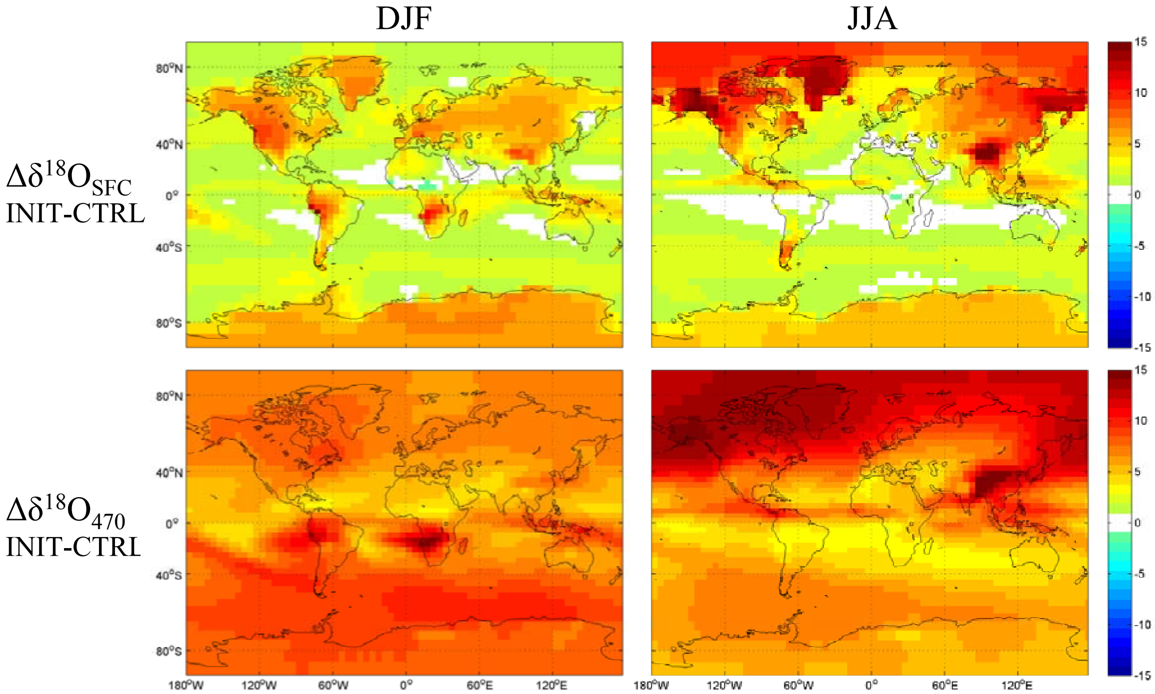

Figure 6. Change in vapor $\delta^{18}O$ composition (‰) for surface vapor and vapor at 470 hPa for INIT.

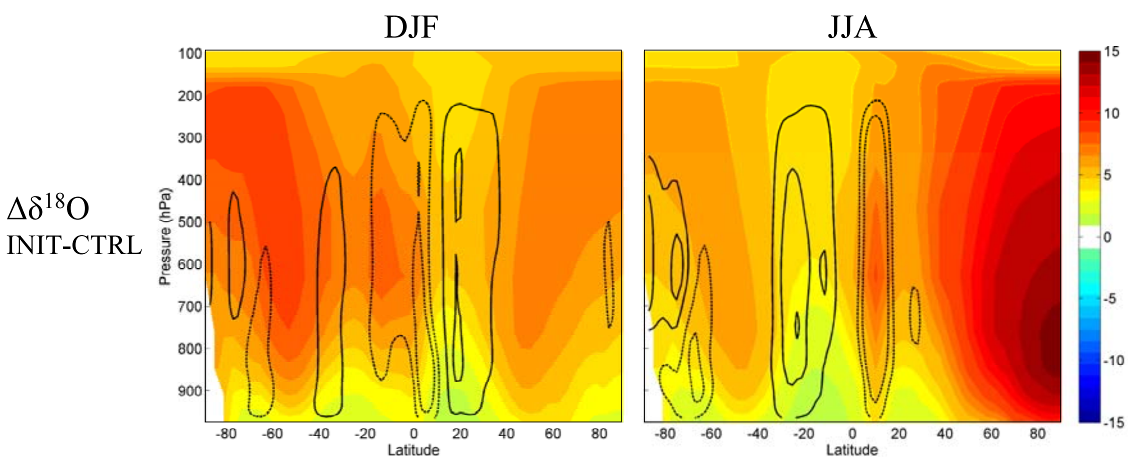

Figure 7. Zonal change in vapor $\delta^{18}O$ (‰) under INIT. Contours show vertical velocity ω (10^{-4} hPa/s), with dashed contours for upward motion (ω < 0), and solid contours for downward motion (ω > 0), each at 1 10^{-3} hPa/s contour intervals.

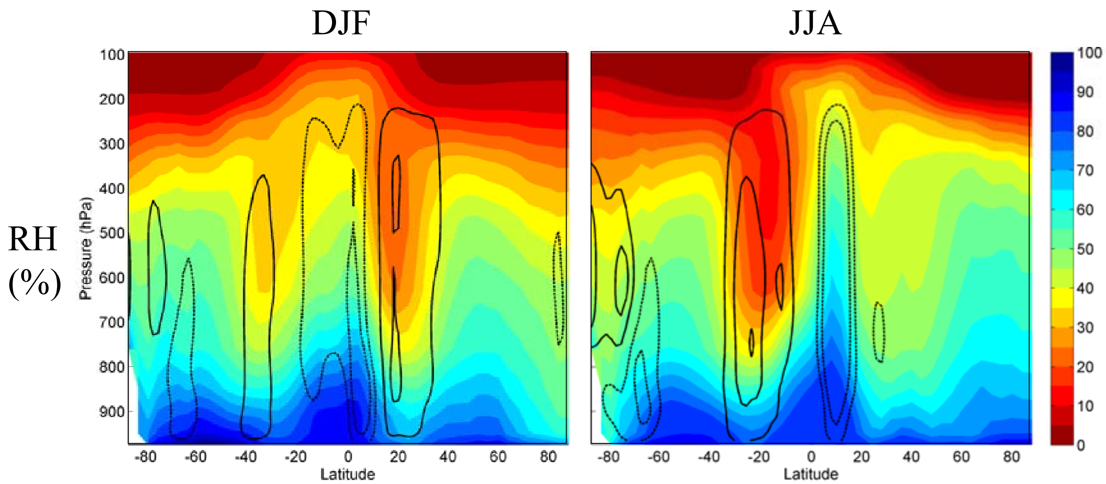

Figure 8. Zonal relative humidity (%). Contours show vertical velocity ω (10^{-4} hPa/s), with dashed contours for upward motion (ω < 0), and solid contours for downward motion (ω > 0), each at 1 10^{-3} hPa/s contour intervals.

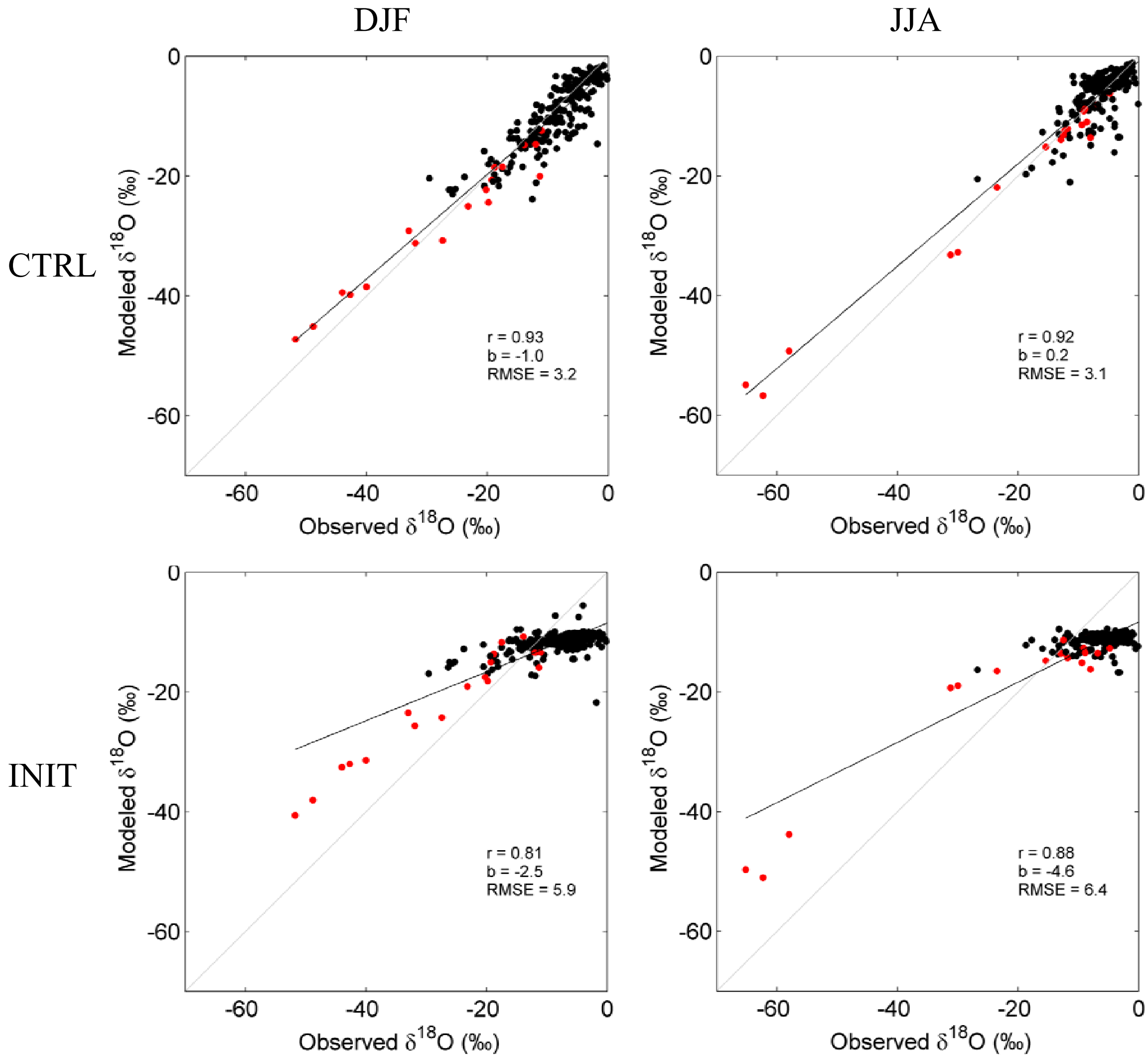

Figure 9. Comparison between observed and modeled precipitation $\delta^{18}O$ for CTRL and INIT with correlation (r), bias (b), and root-mean squared error (RMSE). Observations are for 216 stations in the GNIP database (black circles), with supplemental data (red circles) from Antarctica, Greenland and Russia, as described in the text.

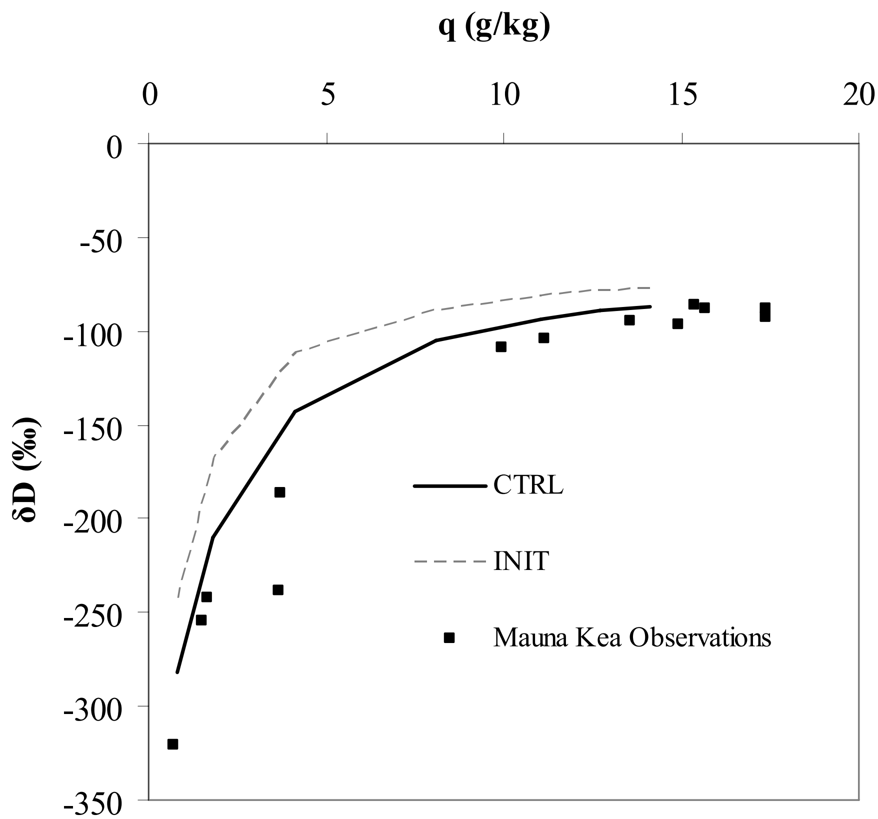

Figure 10. q-δD profiles over Hawaii for CTRL and INIT, with Mauna Kea observations from *Galewsky et al.* [2007]. Measurements were taken between sea-level and 4000m.

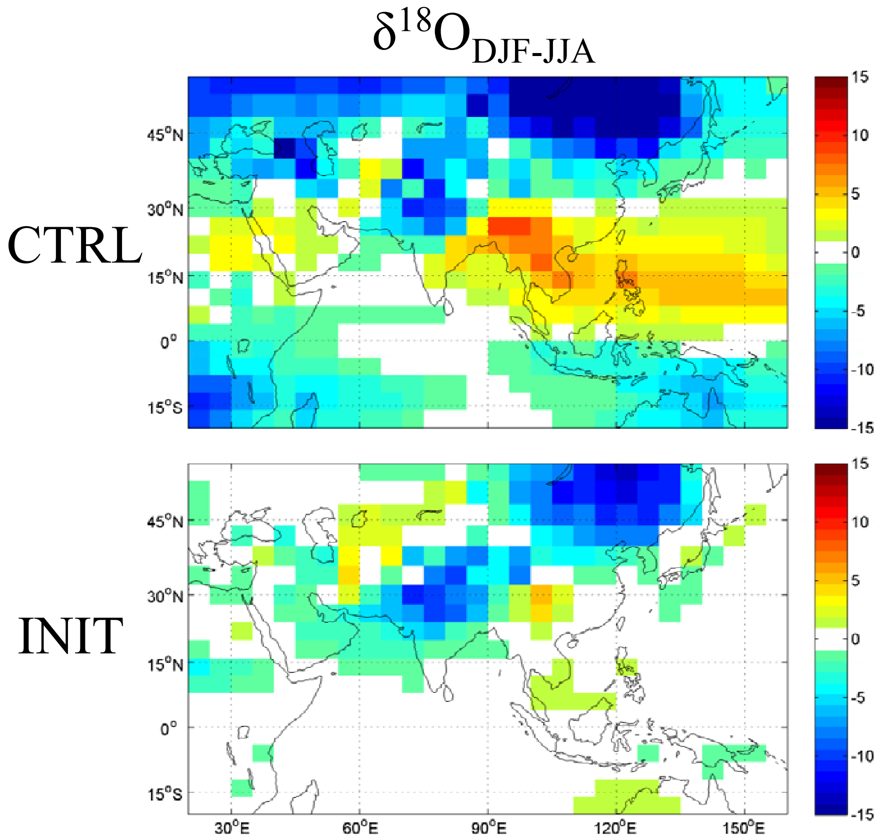

Figure 11. DJF – JJA precipitation $\delta^{18}O$, following *Araguas-Araguas et al.* [1998] and *Vuille et al.* [2005], for CTRL and INIT.

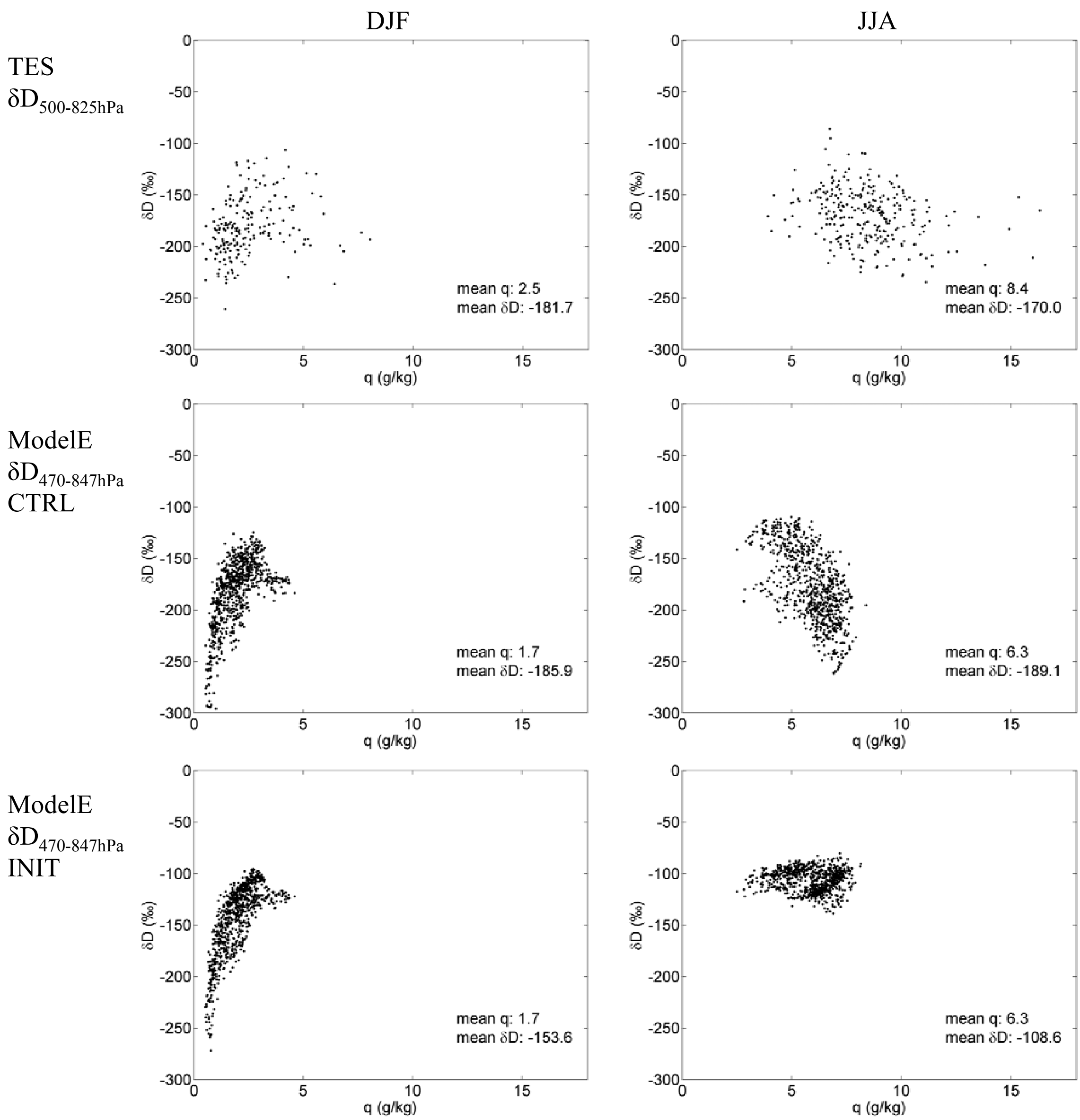

Figure 12. q-δD plots over *Brown et al.'s* [2008] Asian Monsoon region (15-30^{o}N, 80-100^{o}E) for instantaneous TES observations, and mean values from the ModelE CTRL and INIT experiments.

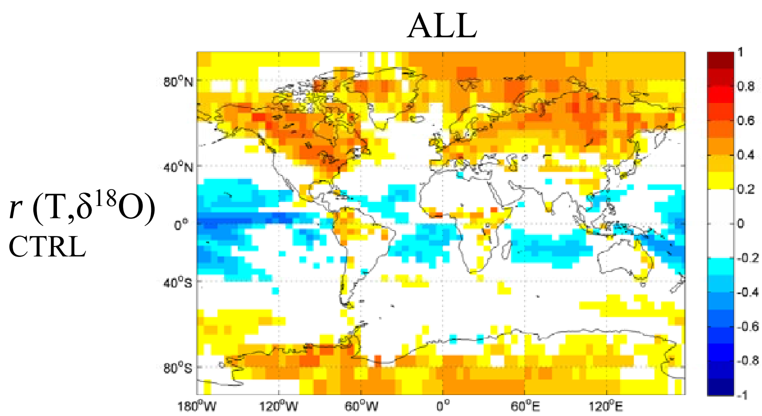

Figure 13. Correlation between monthly surface temperature and precipitation $\delta^{18}O$ anomalies (seasonal cycle removed) for CTRL, during all months of the year.

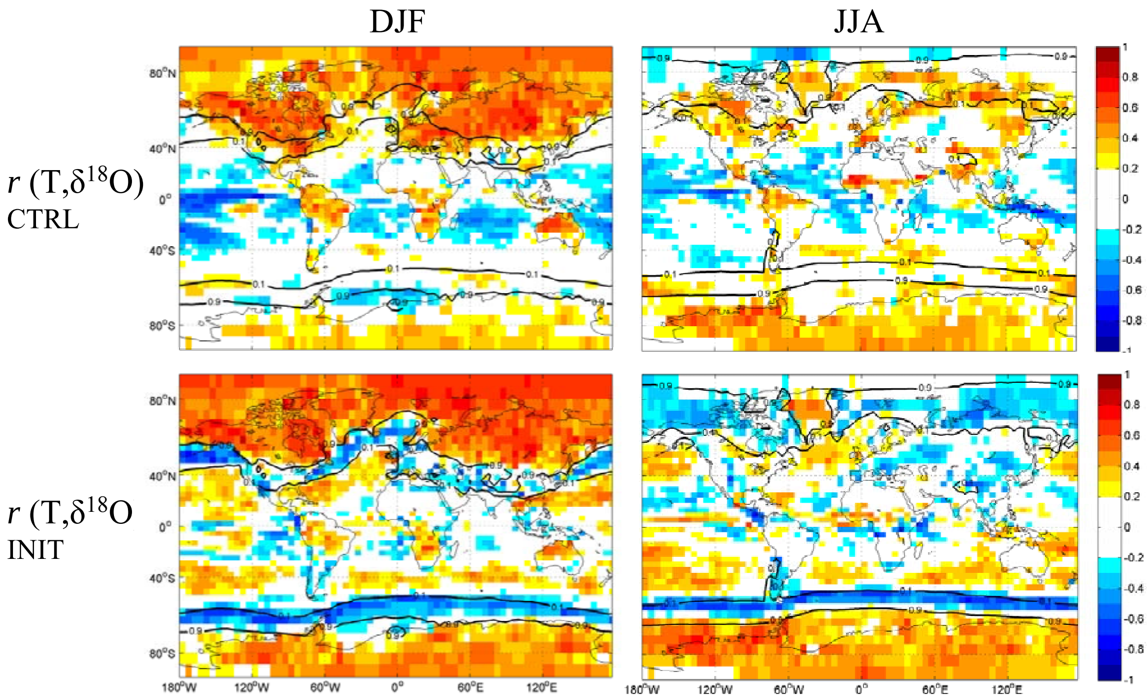

Figure 14. Correlation between surface temperature and precipitation δ^{18}O anomalies for the CTRL and INIT experiments, for different seasons. Black contours show the fraction of precipitation falling as snow at the 0.1 and 0.9 levels.

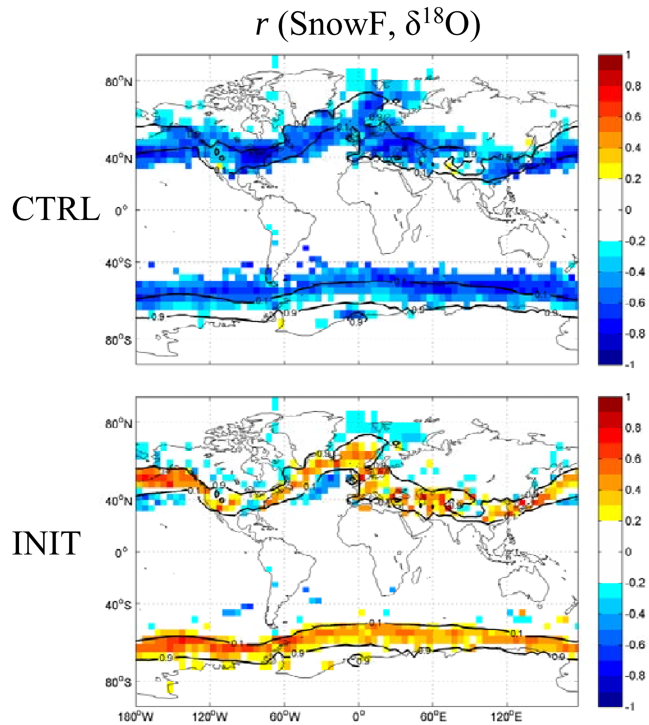

Figure 15. DJF correlation between anomalies of precipitation $\delta^{18}O$ and fraction of precipitation that falls as snow. Black contours show the fraction of precipitation falling as snow at the 0.1 and 0.9 levels.